Investigation of RF Direct Detection Architecture Circuits for Metamaterial Sensor Applications

by

Na'el Suwan

A thesis
presented to the University of Waterloo
in fulfillment of the
thesis requirement for the degree of
Master of Applied Science
in
Electrical and Computer Engineering

Waterloo, Ontario, Canada, 2011

I hereby declare that I am the sole author of this thesis. This is a true copy of the thesis, including any required final revisions, as accepted by my examiners.

I understand that my thesis may be made electronically available to the public.

Abstract

Recent advances in metamaterials research has enabled the development of highly sensitive near-field microwave sensors with unprecedented sensitivity. In this work, we take advantage of the increase in the sensitivity to produce a compact, lightweight, affordable, and accurate measurement system for the applications of microwave imaging and material characterization. This sensitivity enhancement due to the inclusion of metamaterials opens the door for the use of inexpensive microwave components and circuits such as direct detectors while leveraging the high sensitivity of the metamaterial probe to deliver an overall accurate measurement system comparable to that of a traditional probe used in conjunction with a vector network analyzer. The sensor developed is composed of a metamaterial sensor with an RF direct detection circuit. In this work, two prototype measurement systems have been designed and tested. Measurement of small cracks in conductors and material characterization using the proposed system were performed. The results from the newly developed sensors were compared with the results from vector network analyzer measurements. Good agreement was obtained. The feasibility of a compact, lightweight, affordable, and accurate system has been demonstrated by using the developed prototypes.

Acknowledgments

In the name of Allah, most Compassionate, most Merciful.

I would like to thank all the people who made this possible, specially, my supervisor Professor Omar Ramahi for his guidance and interesting questions. I would like to thank my research group Mohammad Al Ramahi, Babak Alavikia, Hussein Attia, Muhammad Boybay, Ali Kabiri, Omar Siddiqui, Zhao Ren, Ali Albishi, Mohammad Alshareef, and specially Mohammed Bait Suwailam.

I would like to thank Zhao Ren and Muhammad Boybay for their help in providing their measurement results for comparison.

For the help in the measurement and equipment, I would like to thank Professor Slim Boumaiza for the access to the EmRG Research group equipments used in the measurements. I would like to thank Nizar Mrabet, Hassan Sarbishaei, and Farouk Mkadem for their help in the EmRG lab. In addition, I would like to thank Professor Raafat Mansour and Mr. Bill Jolley for access and help in the CIRFE lab. In addition, I would like to thank Mr. Nizar Messaoudi for the help in Measurement and access to the microwave lab.

I would like to thank Professor Slim Boumaiza and Professor Mohamed-Yahia Dabbagh for their time in reading this thesis, and their constructive comments and suggestions for the completing this thesis.

I would like to thank my officemate Ehsanollah (Ehsan) Fathi for his help. I would like to thank Salman Kabir for his comments and help on the thesis. I would like to thank Mr. Mohammad Hamdaqa for his comments and suggestions on the thesis.

I would like to thank Mohammad Al Ramahi for his help and assistance in settling in Canada.

I would like to thank my family for their support, patient, and for believing in me; my father and my mother, my brothers (Mo'ath and Mohammad) and my sisters (Nadia, Rima, Rania, and Sarah).

Dedication

And your Lord has decreed that you worship none but Him. And that you be dutiful to your parents. If one of them or both of them attain old age in your life, say not to them a word of disrespect, nor shout at them but address them in terms of honour. And lower unto them the wing of submission and humility through mercy, and say: "My Lord! Bestow on them Your Mercy as they did bring me up when I was young." (The Holly Quran 17:23-24)

I would like to dedicate this for my parents for all what they have given me and asking for nothing in return.

Table of Contents

List of Tables

List of Figures

List of Abbreviations

ADC	Analog to Digital Convert
ADS	Advanced design System
BALUN	balanced-unbalanced
BOM	Bill of Material
CDC	Communication Device Class
CSRR	Complementary Split Ring Resonator
DAQ	Data Acquisition
DC	Direct Current
DUT	Device Under Test
GPIO	General Port Input Output
GUI	Graphical User Interface
IC	Integrated Circuit
ISR	Interrupt Service Routine
LED	Light Emitting Diode
MUM	Material Under Measurement
MUT	Material Under Test
NDT	Nondestructive Testing
NIST	National Institute of Standards and Technology

PC	Personal Computer
RTOS	Real Time Operating System
SMA	Sub-Miniature type A
SPI	Serial Peripheral Interface
SRF	Self Resonant Frequency
SRR	Split Ring Resonator
USB	Universal Serial Bus
VCO	Voltage Controlled Oscillator
VCTCXO	Voltage Controlled/Temperature Compensated Crystal Oscillator
VNA	Vector Network Analyzer

Chapter 1

Introduction

In this chapter, the problems that require compact, lightweight, affordable, and compact measurements systems are highlighted in the problem definition. More concrete examples and motivations for the need for such systems are mentioned in the motivation section. The contribution of this thesis to knowledge is highlighted in the contribution section. Finally, the thesis organization is detailed in the thesis organization section.

1.1 Problem Definition

The search for a compact, lightweight, affordable, and accurate microwave cracks and defects detection system and material characterization and moisture measurement system is needed in multiple industries. Crack detection is needed in airplane maintenance industry [1, 10, 40], the rail track maintenance industry [36], the grain and seeds storage industry [24], and the quality control of material manufacturing industry [13, 26, 15].

Many researchers have shown interest in developing stand alone, accurate and compact sensors. In [13]. In the work of Okamura [26], the emphasis was on size reduction of the measurement fixture by removing the bulky horn antennas with a compact microstrip antennas, and using a small size sensor. Attempts for an inexpensive system have been made by the removal of the expensive vector network analyzer (VNA) and replacing with with a heterodyne radio frequency (RF) detector [26] or by introducing a six-port reflectometer [15]. In this work, we develop a complete stand alone sensor system that is based on RF direct detection (Homodyne) measurement circuit architecture and metamaterials to achieve the requirements of a compact, lightweight, affordable, and accurate microwave measurement system.

The usages of traditional sensors such as open-ended coaxial sensors and loaded waveguide sensors for crack and defect detection have limitations in terms of sensitivity and

resolution. One way to increase the resolution is to increase the frequency, which helps by reducing the diffraction limit of the sensor but this comes with a reduction in the depth resolution as higher frequencies penetrate less into materials. Another method to elevate these limitations of the traditional microwave nondestructive testing (NDT) sensors is by introducing metamaterial which was first suggested in [7]. The improvement in sensitivity and resolution was achieved by using single negative or double negative material in conjunction with the classical NDT probes. The newly designed metamaterial enhanced sensors make possible the fabrication of inexpensive circuits that can achieve good accuracy compared to sensor systems made of traditional probes in conjunction with highly accurate vector network analyzers (VNA). In chapter 3, a microwave NDT measurement system for crack detection was implemented and tested to demonstrate these advantages. By using perturbation theory, the enhancement in resolution and sensitivity can be correlated to enhancement in the permittivity variation, which leads to high-accuracy material characterization. The enhancement in the material characterization was theoretically investigated by the author in [35] using an industry figure of merit to quantify the enhancement for the material measurement application. In this work, metamaterial sensors [32, 9] are used in conjuncture with the systems proposed in this work (Chapter 3 and 4) to deliver a complete measurement system.

1.2 Motivation

It is estimated that the corrosion of airplane parts cost 13 Billion dollars annually in the USA alone[10]. There are many efforts to prevent and to detect surface corrosion. Microwave nondestructive testing (NDT) is for corrosion detection is highly attractive for obvious reasons. The feasibility of the microwave NDT to detect cracks and defects has been investigated exhaustively by NASA in [40], where it has been concluded that microwave NDT is a promising method and can serve the purpose of crack detection. However, the systems proposed in the NASA study [40] are expensive and these systems cannot be extended to all the airplane maintenance industry sectors due to high cost which is an order of tens to hundreds of thousands of dollars per system. In contrast, if a system is available that uses parallel sensing stages, there will be significant money and time savings. Such objective can be satisfied by the phase meter introduced in chapter 3.

Millions of dollars are wasted every year in the grain production cycle due to the post-harvest losses [25]. The losses are due several factors including infestation and microorganism infection. The increase in moisture level in grains is an accurate indication of infestation and microorganism existence. Therefore, the need for an accurate and affordable sensing system to be inserted in every storage bin or to be used by farmers to measure the moisture level of the crops is evident. A continuous monitoring and testing will results

in an early detection of the problems and therefore, early treatment of problems, which leads to a reduction in the post-harvest losses. More than 30% storage post-harvest losses occur in the farms' storage facilities; the farms need an accurate and affordable solution to detect early infestation and microorganism infections. In [24], several methods/sensors for testing the stored crops intended for the reduction of post-harvest losses were proposed and investigated. Highly-accurate methods such as x-ray are very expensive and not available for on-farm storage facilities due to its high cost. The more affordable sensors/systems proposed in [24] such as electric conductance, which is used to determine the moisture level, has a very low success rate of infestation detection compared with the x-ray method [27]. This low success rate is due to the inaccuracy of the electric conductance method to determine the moisture content in the grains. The high accuracy of the system will resolve the problem of poor detection of the infestation and microorganism infection. The moisture content of the grains can be measured accurately from the transmission coefficient amplitude and phase [13]. The Transmission meter system, proposed in chapter 4, can be used to measure the moisture contents of the stored grains/seeds. The affordable price of the proposed transmission meter system (chapter 4), can be adapted by farmers with a fraction of the cost of the available systems [27], while delivering accurate results. The need of a compact, lightweight, affordable, and accurate system is justified by the aforementioned application.

1.3 Contribution

The purpose of this thesis is to develop a stand alone phase and magnitude measurement system to be used in conjunction with a near-field probe. The near-field probe is based on metamaterial technology that enhances the sensitivity of the probe significantly in comparison to traditional probes. The developed RF system will be operating in the low GHz frequency regime in order to maintain inexpensive microwave components. The system is tested on real-world detection problem to demonstrate its utility. The system accuracy was compared to a vector network analyzer and strong agreement was obtained.

1.4 Thesis Organization

The thesis is organized as follows:

Chapter 2: In this chapter, some of the necessary information to complement this thesis are given. The sensors' families of the microwave nondestructive testing (NDT) from the point of view of this study are discussed. Then, the NDT testing applications such as crack detection and material characterization are discussed. The radio frequency direct detection

systems are briefly examined. The existing measurement systems and their limitations are outlined. Finally, the proposed system is discussed, and its philosophy is explored.

Chapter 3: In this chapter, the phase meter for crack detection prototype is discussed and tested. System level design and block diagram are given. The measurement errors in the measurement system are discussed and design consideration to reduce these errors are also outlined. In addition, the calibration algorithms are discussed. The system implementation from a hardware and software point of view are presented. Finally, the measurement setup is shown, and the measurement results are discussed.

Chapter 4: The material measurement prototype solution based on our design proposed system is explored. The system block diagram and high level design details are presented. The detailed analysis of some of the system components used in the system is highlighted. The measurement errors are analyzed, and their effect on the measurement results is reduced by proper design. Finally, measurement and results are analyzed.

Chapter 5: The last chapter provides concluding remarks in addition to suggested future work. The schematics of the transmission meter are given in appendix B, and the μcontroller code used in the design of transmission meter is given in appendix C.

Chapter 2

Background and Proposed Solution

A system of the microwave nondestructive testing (NDT) has mainly two components; the sensor and the measurement circuit. The microwave sensor is a transducer whose functionality is to translate efficiently the electromagnetic interaction with the surrounding material into a circuit measurable quantity. The second component is the measurement circuit whose function is to measure accurately this variation circuit measurable quantity.

In this chapter, we discuss the microwave sensor families; the classical sensors and the metamaterial sensors. The main application of the microwave sensors, in imaging and material characterization, are discussed. The usefulness of using the metamaterial sensors for these applications is highlighted. Then, the radio frequency direct detection is discussed and why it is an exciting alternative for the most common heterodyne architecture for these applications. Before introducing the proposed metamaterial microwave measurement system, a discussion of the existing systems is given in which their limitations and differences from the system are outlined.

2.1 Microwave Sensors

For the purpose of this thesis, microwave sensors are divided into two groups; classical sensors and metamaterial sensors. The metamaterial sensors exploit the inheritance enhancement of the sub-wavelength detection of the perfect lens [28] and this class has been suggested and investigated by [7]. Included in the metamaterial sensor category are inspired by metamaterial sensors such as the sensors in [9, 33].

These two classes of sensors are further divided, from a measurement point of view, into reflection sensors and transmission sensors. This is an appropriate division from this work point of view. There are two microwave measurement systems, which have been designed

and investigated in this work; one for the metamaterial reflection sensors' class (chapter 3) and the other for the transmission metamaterial sensors' class (chapter 4).

2.1.1 Classical Sensors

The classical microwave nondestructive testing (NDT) sensor is a sensor that does not use single or double negative materials in its design. The single negative material refers to a synthetic electromagnetic material where its permittivity or permeability is negative. B permittivity and permeability are negative for the double negative material. The microwave sensor for image detection is a very rich subject, and there is a lot of variation and sensor design dedicated for this application. The use of these sensors had been thoroughly investigated and used in the National Institute of Standards and Technology (NIST) [5]. Sensors can be subdivided into transmission type sensors where the forward transmission coefficient (S_{21}) to give characteristic about the material under test, and into reflection type sensors where the reflection coefficient (S_{11}) is used to get a useful information about the material under test [12].

An example of the setup of the transmission sensors measurement system is shown in Figure 2.1. This setup is composed of two high gain antennas connected to a S_{21}, measurement system such as a vector network analyzer (VNA). The material under test is inserted between these two antennas. From the VNA measurement mainly S_{21}, information is extracted such as permittivity and moisture content of the material under test.

An example of the setup for the reflection sensor is shown in Figure 2.2. This setup is composed of an open-ended coaxial line, which is an example of the reflection sensors. This coaxial sensor is in a close proximity to the material under test. The fringing near field of the open-end will be disturbed by the existence of the material under test. From the measurement of the reflection coefficient S_{11} or its variation (ΔS_{11}) versus displacement the material characteristics and imaging of the material under test can be performed.

For sensing, there are many variations in size, shape, and design of the sensors. There is a rich literature about these sensors; for example, some are using microstrip line for material characterization [39]. However, all of these different sensors can be characterized as either reflection sensors S_{11} or transmission sensors S_{21} or a combination of both.

2.1.2 Metamaterial Sensors

The literature in the electromagnetic theory for the synthesis of a double negative material [34] has exploded in the past ten years. One of the most important features of the negative material is the enhancement of the evanescence field [28], which has been used to enhance the near field sensors [7]. Types of sensors are referred to here as metamaterial

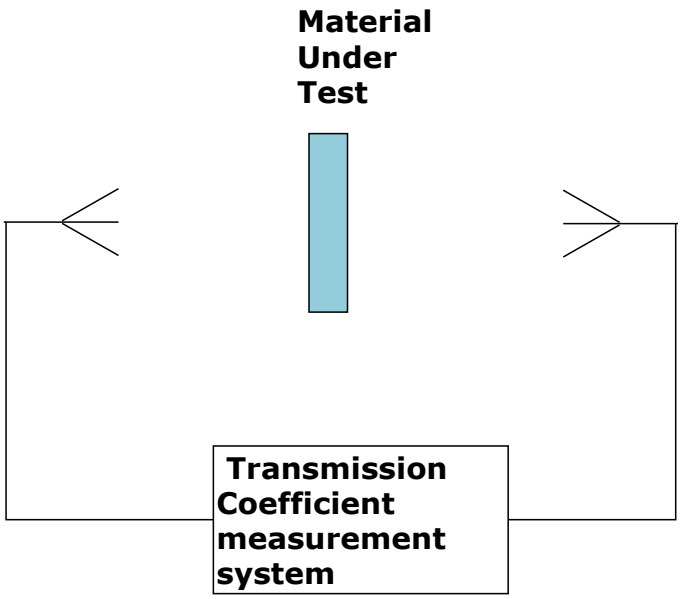

Figure 2.1: Transmission Sensor Setup

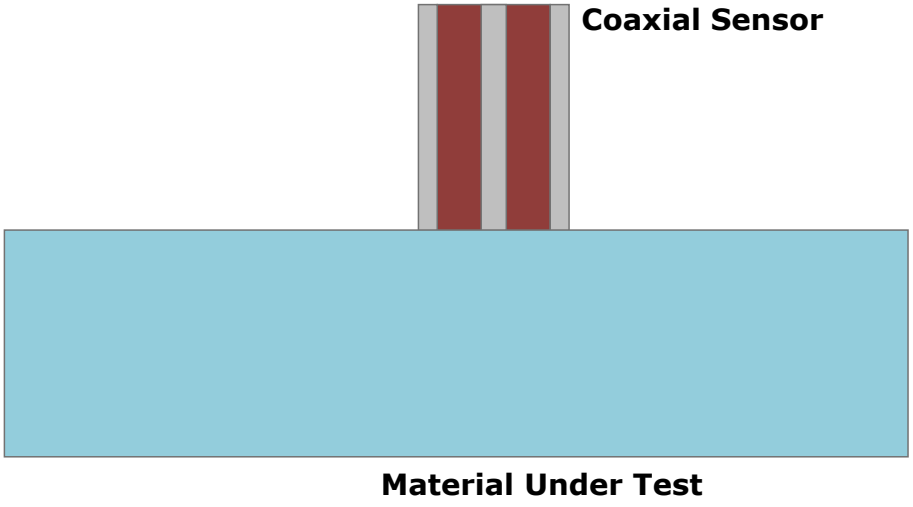

Figure 2.2: Reflection Sensor Setup

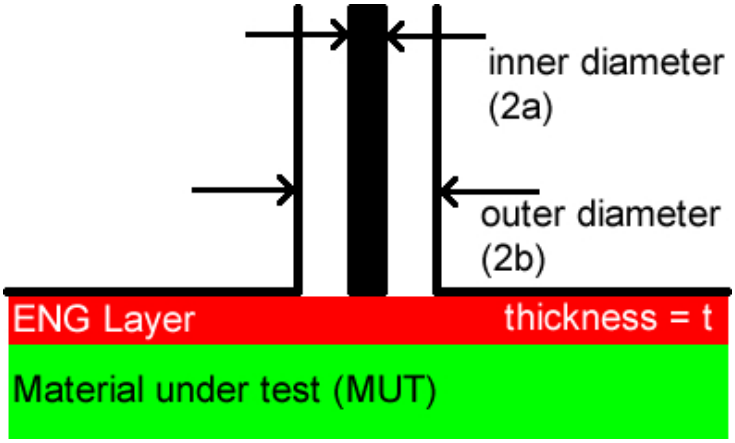

Figure 2.3: ENG-sensor: Metamaterial Sensor Example

sensors to the classical sensor subdivision as the classical. These types can be subdivided into a reflection type such as in [35], or transmission type such as in [9].

An example of the metamaterial sensor is the ENG-sensor shown Figure 2.3[35]. The metamaterial sensor here is based on the open-ended coaxial classical sensor. This classical sensor is the lunch mechanism of the near-field, which interacts with the material under test (MUT). The layer that exists between the MUT and the classical sensor is a metamaterial, which amplifies the near field [28] in order to maximize the effect of material variation on the near-field disturbance. This metamaterial in the optical frequencies range can be a single element such as silver, which has a negative permittivity at the optical frequencies. Moreover, silver has been used as sensor enhancement in the optical frequencies [20].

For microwave frequencies, the metamaterial has not been found in nature. Nonetheless, it has been recently demonstrated that a metallic periodic structure, which utilizes the split ring resonator (SRR) has a negative permittivity around its resonance. This material can be considered as a homogeneous negative permeability material under the condition that the unit cell dimensions is much smaller than the wavelength at the frequency of interest. This structure has been used to demonstrate a synthetic material that have a negative permeability and permittivity [34].

2.2 Nondestructive Microwave Sensors Applications

The nondestructive microwave sensors have many applications including material characterization, moisture measurement, microwave imaging, crack and corrosion detection, and

others. In this section, we focus on two of these applications, in which construct the proposed metamaterial sensing system and test it for these applications. The first application is the crack (groove) detection. This has its application in maintenance of aircraft and the microwave imaging. The second application is related to the material characterization, in which we measure the values of the permittivity of the material under test. This can be extended to figure out the moisture content in the grains, which is useful to grains storage application.

2.2.1 Microwave Imaging for Crack Detection

The enhancement of the evanescent field (amplification) due to a single or double negative material layer in conjunction with a classical sensor [7] and the sub-wavelength imaging resulted from these layer effects [28] has led to the natural conclusion of using this sensor structure as a good subsurface crack detection [8]. From another point of view, this enhancement can be leveraged to relax the requirements on the measurement circuit accuracy in order to achieve a more affordable system with accuracy comparable or better than that of the classical sensor measurement system.

2.2.2 Material Characteristic Measurement

Material characterization using metamaterial sensors has been investigated by the author in [35]. By the knowledge of the enhancement due to the sub-wavelength detection and the knowledge and the understanding of the perturbation theory [38], which can be simply understood by Figure 2.4, the groove (crack) in the system can be replaced by perturbation in the permittivity of the material for small perturbation. So, any enhancement in the imaging system of the cracks can be seen as an enhancement in the detection of the permittivity variation as both changes are similar from the point of view of measurement quantities and field quantities.

The advantage of using a metamaterial sensor for material characterization has been investigated in [35]. An industrial figure of merits for material characterization has been used to demonstrate this enhancement theoretically.

2.3 RF Direct Detection Systems

The most common architecture for a vector radio frequency (RF) measurement circuit is the heterodyne architecture [29]. This architecture is mature and accurate, and it is well understood by designers. In addition, it is the main architecture for most of the commercial

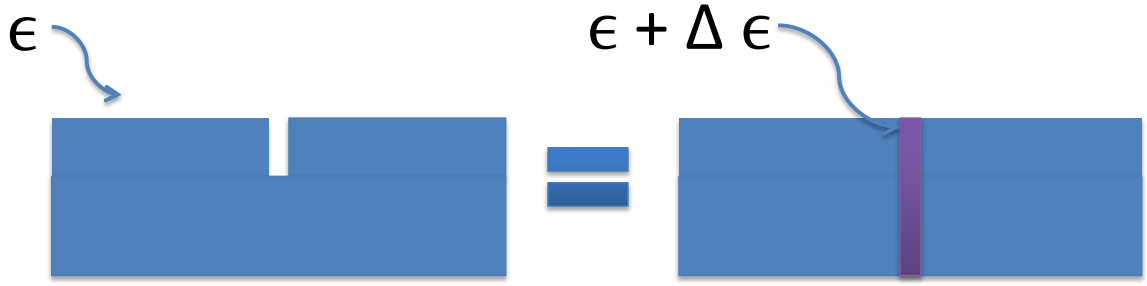

Figure 2.4: Perturbation Theorem and Crack detection

vector network analyzers (VNA) in use today. However, the need for a cheaper VNA has been noticed by many researchers, and smart solutions has been proposed to eliminate the expensive VNA such as six-port reflectometer [14]. In this work, we also exploit the RF direct detection architecture circuit for a more affordable solution for microwave crack detection and material measurement by using metamaterial sensors.

RF direct detection systems are a class of RF circuits, which are used to extract the information content (amplitude and phase) of the high frequency signal using a direct conversion to baseband. This has been investigated thoroughly for the handset wireless industry to reduce cost, components count, and power consumption [31]. Included in this category is the six-port vector network analyzer [16] as it uses a direct conversion from radio frequency to direct current (DC). There are a lot of challenges in the RF direct detection (homodyne system) [19, 30, 17]. However, the benefits of using such a system are more rewarding than the trouble of designing it to overcome the accuracy limitation.

2.4 Current Sensor Measurement Systems

In this section, previous attempts to get a compact and a more affordable system are discussed, and their benefits and limitation are highlighted.

The system proposed in [15] uses a six-port reflectometer for the measurement of the permittivity of the material under test. The simplicity and versatility of the six-port reflectometer in microwave application [16] would normally attract researchers to implement it in material characterization applications as a replacement of the vector network analyzer (VNA) for a permittivity measurement solution. However, the system in this paper failed to address the compactness and affordability as it uses lab equipments such as HP 8620C

sweep oscillator in its measurement system. This system surely is more affordable than its VNA alternative; even though, it is still expensive.

Another interesting attempt to design an affordable microwave nondestructive testing (NDT) crack detection system based on the six-port reflectometer variation has been proposed in [1]. The usage of high frequency (X-band) allows a small resolution for the detection of small cracks. The microwave imaging resolution is normally limited by the diffraction limit. However, this will impose a very high cost to the synthesizer system as we increase the frequency where its cost is proportional to the used frequency. The system has been implemented using a lab equipment to demonstrate the feasibility of the usable system. As the smallest image resolution is bounded by the diffraction limit, which is a function of the wavelength, this limits our image resolution for all electromagnetic imaging systems. By introducing the metamaterial in the sensor, the diffraction limit is not the smallest resolution of the microwave image, and this is referred as sub-wavelength imaging. This is analyzed and proved by Pendry in [28]. The introduction of metamaterial in our system enables even a lower cost system by using lower frequency circuits while not sacrificing the resolution.

Reducing the size of the test fixture is another way to reduce the size of the measurement system and lower its cost. The attempt to produce an affordable and more compact system by fixture reduction is performed in [13]. In the standard accurate system for moisture measurement, high directivity antennas are needed for the transmission measurement method for moisture measurement. It has been an industrial standard to use horn antennas for this purpose. In [13], horn antennas used in the measurement system sensors intended for moisture measurement has been replaced by more compact and cheap microstrip antenna arrays. However, this design still uses the expensive network analyzer as a measurement instrument, which hinders the adaptation of such systems by other industries where the cost is more sensitive.

The reduction of the size of the sensor and usage of material measurement circuits has been performed in [26]. Attempts has been made to reduce the size of the sensors while reducing the cost by using a simple microstrip line as a transmission line sensor [26]. This circuit is using a double heterodyne measurement architecture circuit, and then it performs a baseband processing to generate the phase and amplitude difference to get the proper moisture content measurement. This system was optimized for the accuracy while sacrificing the cost by using two heterodyne at the frequency of operation, compared to the more affordable homodyne (direct conversion) systems, which is used here. In addition, the lack to leverage the enhancement of the metamaterial sensors, which this work does, is a drawback as a more accurate system can be produced by leveraging the sub-wavelength image resolution and detection using the metamaterial sensor.

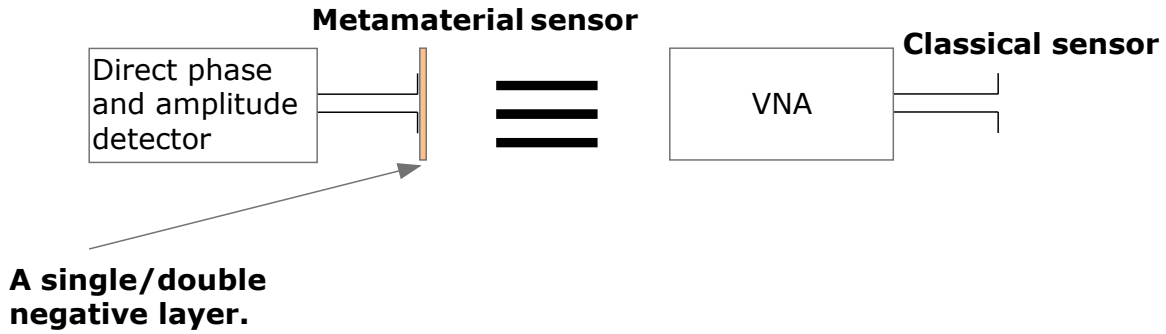

Figure 2.5: Performance Equivalence Between Proposed and Existing System

2.5 Proposed Metamaterial Measurement System

The metamaterial measurement system, which is proposed in this work, combines the enhancement of the metamaterial (evanescent field amplification) with an affordable direct detection microwave circuit. This is done in order to achieve a comparable system performance to a heterodyne detector (such as a vector network analyzer) with the classical type of microwave sensor. This relationship can be seen as an equivalent between the system proposed and the existing classical system in terms of performance as illustrated in Figure 2.5. Nonetheless, our proposed system is more affordable.

To demonstrate the benefits from this combination of a metamaterial sensor and direct detection circuits, two systems have been investigated and built. One is the phase meter system (chapter 3), which is a direct conversion of a saturated reflected signal to produce a DC signal, which its level is proportional to the phase difference between the incident and reflected wave from the sensor. This system is shown to be compact, lightweight, affordable, and accurate for crack detection application. A data acquisition (DAQ) card is used to measure the DC voltage from the output of the circuit. A computer is used as an interface to collect the measurement data, which can be replaced by a μcontroller for detection and reporting algorithm.

The second proposed system for material characterization (chapter 4) is also based on the direct detection. In this system, we propose the usage of a direct detection integrated circuit (IC) from analog devices (AD8302). This enables us to measure the amplitude and the phase between the transmitted signal and the reference signal. The knowledge of the complex transmission coefficient is more useful than the scalar transmission coefficient, as it provides additional information, which can be used in complex permittivity or determining

the moisture content of a composite material.

The performance of the proposed system is compared with its equivalence, which is shown in Figure 2.5. The measured data evaluated is the permittivity of a reference material under test. This has been done as the ultimate goal of the system is to measure material characterization and detect cracks. As there is no previous system that uses the metamaterial sensors for the creation of a compact, lightweight, affordable, and accurate system, this seemed as the natural approach for validating the proposed measurement system.

Chapter 3

Phase Meter

In this chapter, a phase meter system, which is a device used to measure the phase of the reflection coefficient (S_{11}) using a direct detection architecture, has been designed and implemented. The phase meter has been tested with a metamaterial sensor for crack detection application. This device direct conversion architecture simplifies the design and provides a more affordable metamaterial measurement system. In addition, the use of a metamaterial sensor enhances the performance of the overall measurement system.

3.1 Introduction

The design of a compact, lightweight, affordable, and accurate sensing system for crack detection application is explored in this chapter. The main focus of this chapter is the design of this microwave measurement circuit in order to use the inspired metamaterial sensor mentioned in section 2.1.2 to achieve a better microwave measurement system.

3.2 System Level Design and Block Diagram

A system level diagram is shown in Figure 3.1. The system is based upon two-coupler reflectometer architecture where its limitation and error model is thoroughly explained in section 2.7 of "Principles of Microwave Measurements" [11].

The design frequency of interest of the system is 1.2 GHz, which is the design frequency of the metamaterial sensor [33]. In this design, we have used a voltage controlled oscillator (VCO). This VCO is controlled by a voltage divider through a potentiometer to set the center frequency. The design is based on a direct conversion of the reflected signal from

the sensor connected to the measurement device. The reflected signal is amplified until saturation. This makes the DC signal dependent only on the phase variation of the reflected wave and not its amplitude. The signal is then mixed with the reference signal of the system and down converted into DC. The resulting DC signal is post-processed by an amplifier, and it is read by a data acquisition (DAQ) card and mathematically converted to get the proper phase reading.

In Figure 3.1, port one, two, and three are connected to the radio frequency source, sensor, and the DAQ, respectively. The signal is traveling from port one toward port two while it is being coupled by the first directional coupler as a reference signal. The reflected signal from the sensor, port two, is coupled using the second directional coupler, as a test signal. The test signal is then amplified until saturation, so that the output signal will be only dependent on the phase difference of the two signals; the reference and the test signal. Both the saturated test signal and the reference signal are mixed and converted into a DC signal proportional to the phase difference of the reflected wave.

This DC signal is post-processed and filtered, which is being read by the DAQ. A computer software is used to convert the raw data from the DAQ into an actual phase variation using the phase data calibration in the system. A calibration algorithm has been used to relate the measurement of the DC voltage readings to the phase of the reflected signal. The reading of the DC signal has been done using the implementation of the serial port communication class, implemented in Microsoft Visual Studio library, to communicate with the DAQ card. Finally, some results are given and discussed.

3.2.1 Ideal System Analysis

In this section, the system will be analyzed assuming an ideal system, which means the directivity is infinity and there is no mismatch between the system components. Assuming the test signal is $A_{test}\cos(\omega t)$, and the reference signal is $A_{ref}\cos(\omega t + \theta)$. If we analyze the ideal system ignoring the amplification of the test signal (this is done to understand the need for saturating the test signal) the mixer output will be simply as

$$\frac{A_{test}A_{ref}}{2}\cos(2\omega t + \theta) + \frac{A_{test}A_{ref}}{2}\cos(\theta) \tag{3.1}$$

The first term of the equation 3.1 is ignored as the output of the system will be filtered by a low pass post-processing filter. The second term is a DC signal which is dependent on both the reflected wave amplitude from the sensor due to the A_{ref} and the phase of the reflected wave (θ). The input signal amplitude is a constant in our system; so, its value does not affect our mixer output under ideal system conditions. The DC signal value will have an ambiguity in its variations, due to the reflection coefficient amplitude and the phase.

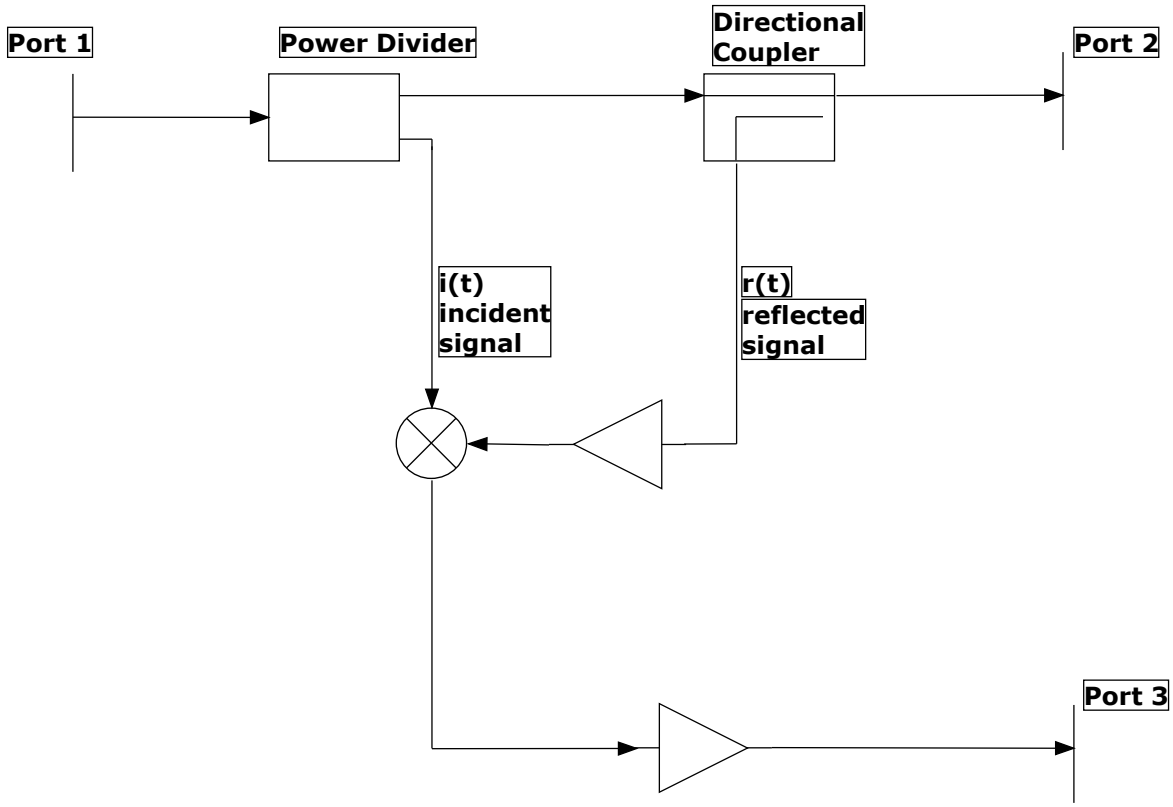

Figure 3.1: System Level Blocks of the Phase Meter Measurement System

To solve this ambiguity problem, we need to neutralize the amplitude dependence effect on the output signal, by adding an amplifier in the path of the test signal and making sure that the amplification level will cause the test signal to saturate by a large amplification margin. Then, we can say that the low pass signal from the mixer, assuming the effect of the saturation, is as follows

$$\frac{A_{test}\mathrm{TF}(A_{ref}\cos(\theta))}{2} \tag{3.2}$$

where TF is a hard-limit transfer function of the signal amplitude which relates the output saturated test signal of the amplifier to its input signal. The saturation is a nonlinear process on the signal, and it will distort the signal into a square wave by introducing the nonlinear hard-limit. The analysis here is to understand the system behavior and architecture. If the TF causes the system into deep saturation then the amplified reflected signal can be modeled as a square wave with a constant peak to peak. By introducing the amplifier to the system, the DC output will be insensitive to the variation in the amplitude of the reflected wave, and it will only be sensitive to the phase variation.

To find the dynamic range of the system assuming an ideal system, we need to analyze the signal power levels. If Γ_{sens} is the reflection coefficient of the sensor, P_{in} is the signal input power, C is the coupling coefficient of the coupler, P_{sat} is the saturation power level of the amplifier, and G is the gain of the amplifier. The output power level at the input at the mixer from the reflected signal side can be calculated as $P_{MT} = P_{in}\Gamma_{sens}G/C$. To ensure a hard saturation level we must have $P_{MT} >> P_{sat}$.

The dynamic range in dB of the system is calculated by

$$P_{in} + \Gamma_{sens} - C + G > P_{sat} + 10\mathrm{dB}$$

which is rearranged to give

$$\Gamma_{sens} > P_{sat} + 10\mathrm{dB} - P_{in} + C - G \tag{3.3}$$

From equation 3.3, the limit of the minimum reflection coefficient of the sensor, which can be measured accurately using our system is given. For our system, P_{in} is 0.5 dBm, P_{sat} is 18 dBm, C is 6 dB, and G is designed to be 60 dB. The minimum measured reflection coefficient that will not affect our system accuracy is -29.5 dB. This is good for our practical considerations. Of course, we can increase the gain of our system. However, this will be at the risk of system instability and oscillation, due to unintentional positive feedback from parasitic elements between the input and the output and other coupling paths.

3.2.2 System Measurement Errors

The implementation of the system as mentioned above introduces measurement errors. The first three errors, mentioned below, which are common in the reflectometer systems as found in section 2.8 of "Principles of Microwave Measurements" [11], while the remaining errors are related to this system particular design. The errors are as follows:

1. Directivity Error: This is due to the finite directivity of the used couplers. For this reason, the couplers used in this prototype to implement a reflection bridge are transformer type coupler with an excellent isolation [22].

2. Transmission Error: This is due to the mismatching on the transmission line path and the coupling losses which causes a mismatch. The design of matched transmission lines to 50 Ohm in the system reduces the mismatch between different components.

3. Effective Source Error: This is due to the mismatch of the input port looking into the phase meter. This is referred to the effective source error because this reflection error is affected by the coupled signal from the directional coupler which is the directivity of the coupler.

4. Harmonic Variation Error: As it has been mentioned in section 3.2.1, the test signal is saturated in order to cancel the dependence of the DC output signal on the system. To reduce this error, the system is always ensured to be working on the deep saturation region where the variation of the reflection coefficient of the sensor will have a negligible effect on the system.

5. Oscillator Frequency Control Error: As the frequency output is controlled by a potentiometer, the system has random errors of frequency shifting and drift from the nominal frequency of operation and calibration. This shift is kept to a minimum by re-tuning the system before every measurement. There is nothing that we can do in our system except for the consistent calibration to the system, and this should be introduced in the next version of this phase meter.

3.3 Calibration Algorithm

The calibration of this system is performed by using three transmission line extensions between the port and the sensor. These extensions are normal Sub-miniature type A (SMA) adapters that have been characterized by the Vector Network analyzer (VNA). The phase versus frequencies data has been stored to be used by the software in the calibration algorithm. Three extensions have been used to characterize the conversion between the

voltage shift and the phase shift, in addition to the removal of the ambiguity of the phase sign. The removal of the phase shift ambiguity increases the range of the phase measured from 180° to 360°.

As our system concentrates only on the measurements of relative phase shift, the previous calibration procedure is suitable for our purposes.

3.4 System Implementation

The phase meter system has been prototyped as a proof of concept on FR-4 prototype board. There has been a mismatch of the system due to the parasitics and non-ideal transmission line. However, as a prove of concept design the prototype has shown a lot of potentials. The design is shown in Figure 3.2.

3.4.1 Hardware Implementation

The implemented hardware components are shown in the Figure 3.2. The subsystems are highlighted on the figure. There are three external components for this system, the power supply which is a 9 V battery, the sensor which is used in [33] connected to the coaxial line, and the data acquisition (DAQ) controller from DLP design, Inc (DLP-IO8-G).

The system components are shown in the figure are as follows: Voltage Controlled Oscillator (VCO), the power divider which is used as a refractometer bridge, the cascaded amplifiers, the Mixer, the OP-AMP, which is a rail-to-tail op-amp used for signal level shifting and amplification, and the voltage regulator which is used to regulate the 9 V power supply to 5 V. The components are summarized in Table 3.1.

Component	Manufacturer	Components part Number
VCO	Mini-circuits	ROS-1250W-119+
Power Divider	Mini-circuits	SBTC-2-15-75L+
Voltage Regulator	497-7758-1-ND	KF50B
OP-AMP	Microchip	MCP6V01/2/3
MIXER	Mini-circuits	MACA-242H+
Amplifiers	Mini-circuits	ERA-50SM+ as signal amplifier MAR-6SM+ as a final stage amplifier
Potentiometer	BOURNS	3590P-2-103L

Table 3.1: Main Components used in the Phase Meter

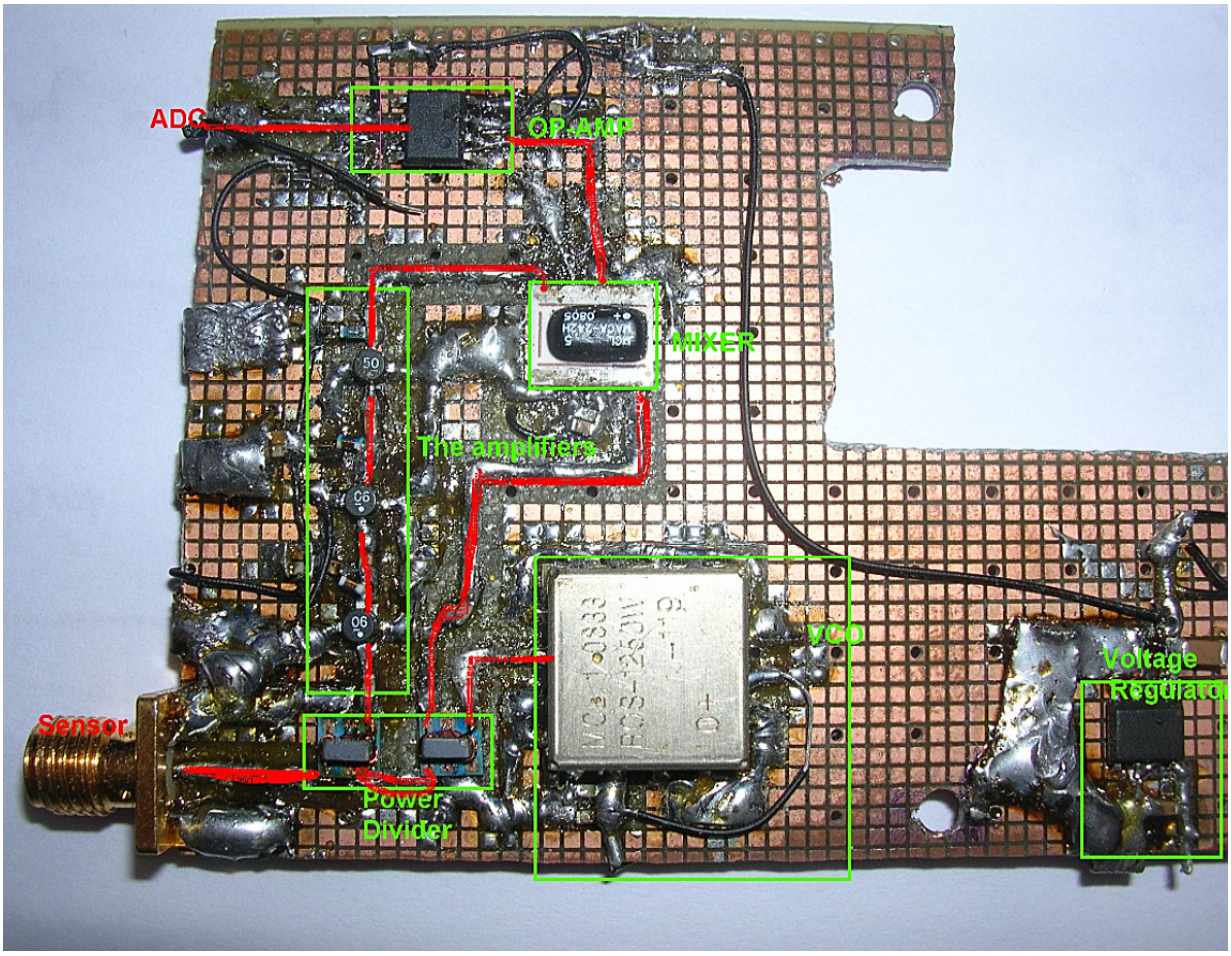

Figure 3.2: Phase Meter Prototype

3.4.2 PC Software Interface Implementation

The Software implementation for this part is mainly on the personal computer (PC)! side. The software interface has been implemented in C# and Visual studio libraries. The serial port communication class has been used to interface with the data acquisition (DAQ) card from DLP Design, Inc, as a virtual serial port over Universal Serial Bus (USB). The functionality of the DAQ has been wrapped using a wrapper class in order to simplify the communication between the software and the DAQ. The detection of the serial port has been implemented automatically for simplification of the operation on the user.

The Graphical User Interface (GUI) implemented for the phase meter measurement system is shown in Figure 3.3. There are two GUI interfaces; one is used as a configuration and calibration 3.3(a), and the other is used for measurement reading 3.3(b).

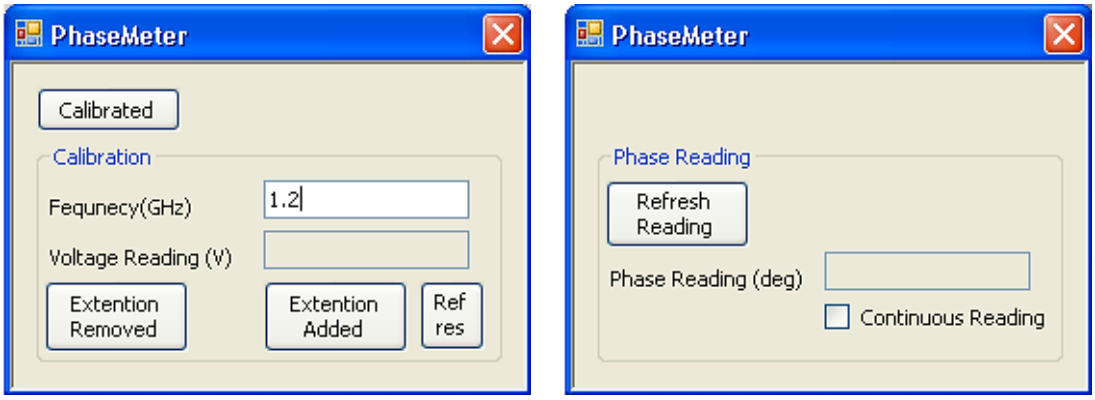

(a) The Calibration GUI (b) The Measurement GUI

Figure 3.3: Software GUI for the Phase Meter

In the calibration interface Figure 3.3(a), the program requires the user to provide the frequency of the operation. This information can be found using a spectrum analyzer after potentiometer tuning. The calibration is performed with the sensor connected by varying the transmission line length. The transmission line is varied by cascading one or more Sub-miniature type A (SMA) adapters. The physical change of the system is done as a hardware, and then by pressing the appropriate buttons the system interface will save the voltages and use them in combination with the stored information about the adapters extension versus frequency to determine the proper change in voltage to convert it into phase readings. In addition, the raw voltage reading is shown in the GUI in order to have a debugging and a fault indication mechanism.

The measurement interface as shown in Figure 3.3(b) is very straight forward. It will show the reading of the phase assuming the calibration reading is done at a zero degree. There are two modes for phase reading one of the modes is where a user request the reading by pressing the *Refresh Reading* button. This is the default mode. The second mode, in which the program continuously polls the updated phase readings every one tenth of a second, is chosen by selecting the *Continuous Reading* check box in the GUI.

3.5 Measurement Setup and Results

The setup used in this measurement is the same the one used in [32]. The only difference is that the measurement performed here for a non-lossy material(i.e. Air). The setup is composed of a station with the metamaterial sensor at the base of it, and an aluminum cube which has a 3D freedom movement with a fine displacement down to 1 mm.

Figure 3.4 shows a comparison between the measurement of the system provided by the author of [32] used a Vector Network Analyzer (VNA) and the measurements done by using the phase meter system. Both measured data sets have been normalized by the maximum value measured far away from the 20 mm by 20 mm Aluminum test cube. The measurement results of the VNA have 1 mm displacement, while the phase meter results are discrete values in the step of the cuboid and away from it. The agreement between the two measurement systems is good. The variations and error can be attributed to the errors in finding the exact location when repeating the experiment.

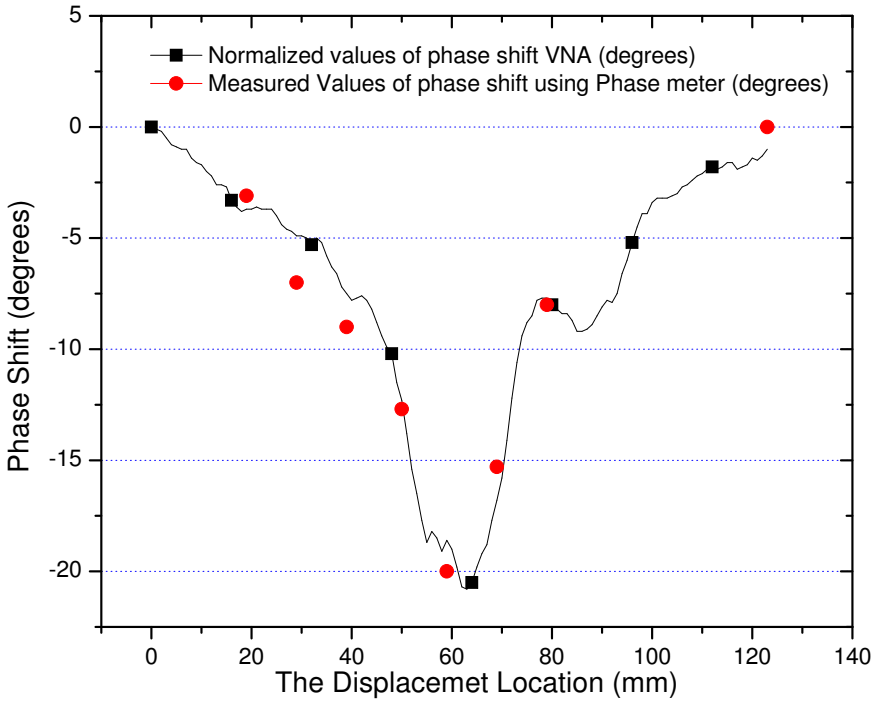

Figure 3.4: Phase Meter Measurement Comparison

The system has a poor absolute phase value accuracy even with the proper calibration discussed. However, the matching of the results in a relative phase measurement makes this system be a good candidate for test systems of crack detection were only ON/OFF (TRUE/FALSE) detection is needed.

3.6 Conclusion

In this chapter, the design of a phase meter prototype system based on direct architecture detection has been demonstrated. The issues of design have been addressed, in addition to the treatment of error sources. Finally, a comparison has been performed using a metamaterial sensor, in which the data has been illustrated this prototype design is an adequate for TRUE/FALSE type tests. This TRUE/FALSE type test is suitable for the application of crack detection or fault detection in manufacturing and maintenance applications.

Chapter 4

Transmission Meter

4.1 Introduction

The need for an affordable portable material characterization system is a necessity for industrial application. In this chapter, the focus is on the design of the transmission meter, which is used for the measurement of a forward transmission coefficient (S_{21}). The architecture for the meter is based on the direct detection architecture, which is based on the Analog device's integrated circuit (IC) (i.e. AD8302)[2]. This architecture grantees a good resolution of the material characterization, and this resolution is suitable for usage with the metamaterial sensors family. The sensor that is used for evaluation of the system is analyzed and studied [9].

This chapter starts with a system level overview and block diagram of the transmission system. Then, the error model and the system calibration algorithm are discussed. Next, several components implementations of the systems have been discussed from both the hardware and the software point of view. In the last section, the measurement results of the transmission meter are presented in order test its functionality for material characterization application. The results from the transmission system are compared with the results from Vector Network Analyzer (VNA). A practical application to measure the permittivity of material is implemented to demonstrate the system use for material characterization applications.

4.2 System Level Overview and Block Diagram of Transmission Meter System

The transmission meter measurement system, shown in Figure 4.1, is composed of five main components: the μcontroller with the power distribution network, the oscillator subsystem, the amplitude and phase meter subsystem, the power coupling and isolator network, and the switched phase shifter network.

The μcontroller is used to interface with the different subsystems on the board and to communicate with a computer through Universal Serial Bus (USB) port. This muController interface includes the analog to digital conversion of the baseband voltage corresponding to the phase and amplitude of the radio frequency from the amplitude and phase meter subsystem. The DC power for this measurement device is supplied by DC voltage of the USB port. The oscillator subsystem is used to sweep over the desired frequency of operation (700 MHz up to 1300 MHz) with a 500 kHz step size. The amplitude and phase meter subsystem is used to directly convert the radio frequency signals from the transmitter and the receiver ports to give two DC signals, which are proportional to the amplitude difference and the phase difference between the two radio frequency signals. The coupling network is used to couple the signal from the oscillator into the amplitude and phase subsystem. Meanwhile, the isolator network isolates the reflected signal due to the mismatch of the device under test (DUT), such as metamaterial sensors, from the input port. The phase switching network is used to change the phase of the signal path by a calibrated value in order to increase the accuracy of the phase and amplitude measurement network as the amplitude and phase meter subsystem has a high error when the two signals phase differences are in-phase (zero phase difference) due to the AD8302 accuracy limitations.

4.3 Error Model and Calibration Algorithm

To minimize the errors in the transmission measurement system, we need to investigate the error model of it. The reduction of the measurement errors, phase and amplitude, to an acceptable tolerances is performed by both design and calibration consideration. The error model and calibration of a similar measurement systems has been thoroughly investigated in Bryant book [11], and this can be extended to this work.

The Error Model

The measurement of the normalized transmission parameter is done by normalizing the measurements with device under test (DUT) to the measurement without the DUT. The

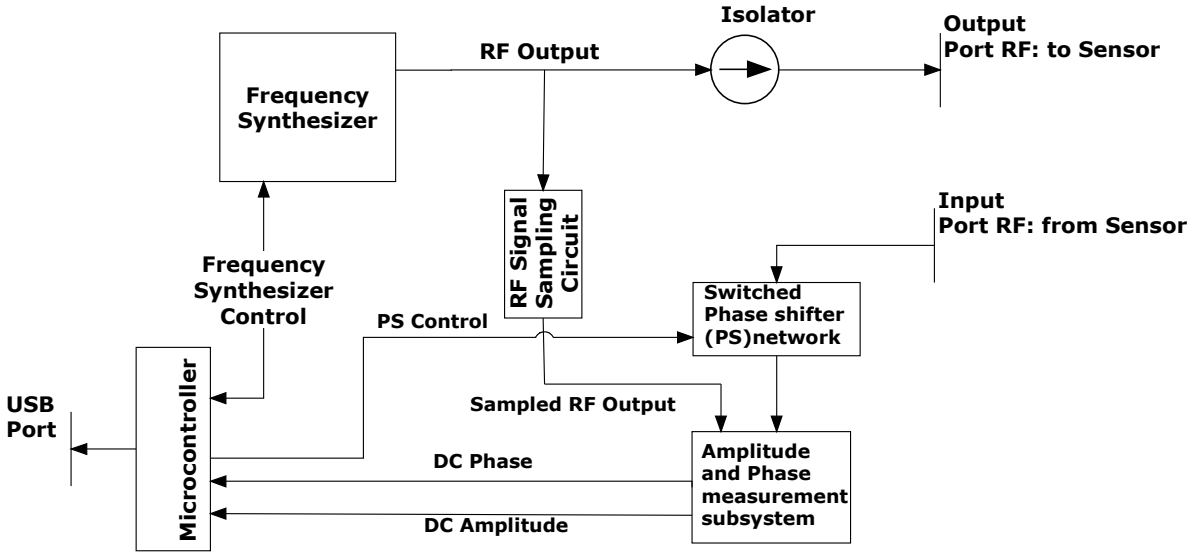

Figure 4.1: Top Level Schematic of the Transmission Meter System

error analysis from section 2.6 in "Principles of Microwave Measurements"[11] can be extended to our system by adding an isolator and a transmission line extension after the power tap coupler.the system without the DUT becomes as shown in Figure 4.2, and the system with DUT becomes as shown in Figure 4.3. The equation 4.1 of the error can be derived as shown in Appendix A from the two signal flow graphs shown in Figure 4.3 and 4.2 as follows:

$$S_{21M} = \frac{S_{21}(1 - K\Gamma_{PT}\Gamma_{Mckt})}{1 - K\Gamma_{PT}\Gamma_{DUTin} - KS_{21}\Gamma_{PT}S_{12}\Gamma_o^2 - \Gamma_o^2 + K\Gamma_{PT}^2\Gamma_{DUTin}e^{-\gamma l}S_{21}S_{12}\Gamma_o^2} \tag{4.1}$$

where $K = \text{Iso}e^{-\gamma l}$ and $\Gamma_o^2 = \Gamma_{DUTin}\Gamma_{Mckt}$

In equation 4.1, S_{21M} refers to the measured transmission parameter, where S_{21} refers to the actual transmission coefficient of the DUT. The reflection coefficients of Γ_{PT}, Γ_{Mckt}, $\Gamma_{DUT_{in}}$, and $\Gamma_{DUT_{out}}$ are power tap, measurement circuit input, DUT input, and DUT output reflection coefficients, respectively. The parameter l is the physical length of the transmission line, and γ is the propagation constant of the transmission line.

By maximizing the isolation of the isolator (Iso$\rightarrow$0), some error components can be reduced, and the equation 4.1 reduces to $S_{21M} = S_{21}/(1 - \Gamma_o^2)$, where $\Gamma_o^2 = \Gamma_{DUTin}\Gamma_{Mckt}$. The final equation error is dependent on the input reflection coefficients of the input DUT

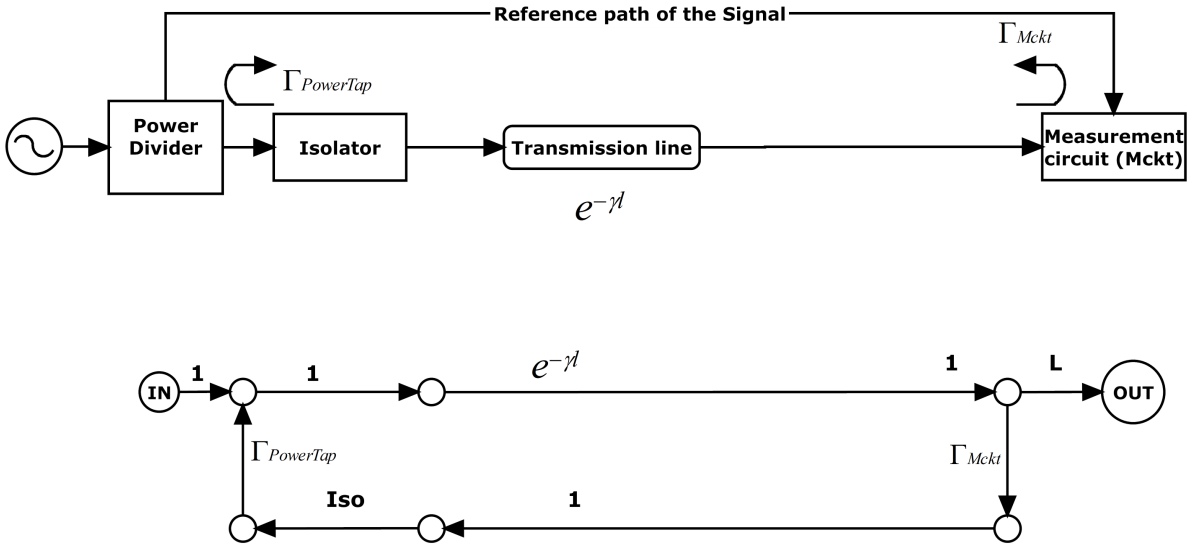

Figure 4.2: Error Model Analysis Without the Device Under Test (DUT): the System and the Signal Flow Graph

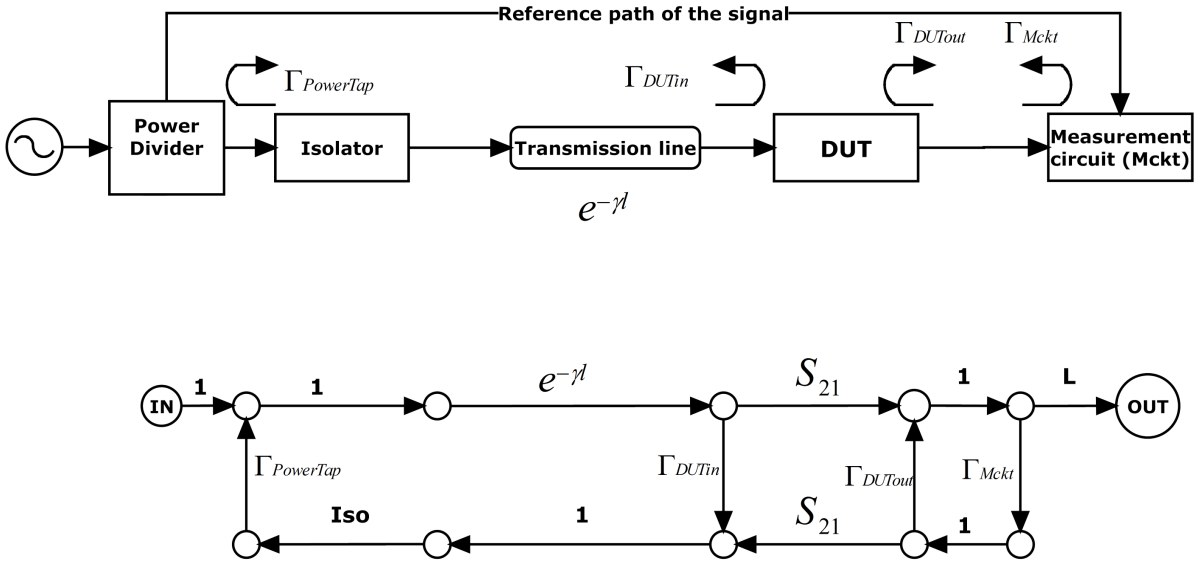

Figure 4.3: Error Model Analysis with the Device Under Test (DUT): the System and the Signal Flow Graph

and the input measurement circuit. The using of an isolator is beneficial for error reduction and control. However, for a broadband system such as ours, there is a problem in finding a compact and an affordable microwave isolator. This problem is elevated by substituting an isolator by an attenuator in our prototype. For an attenuator instead of isolator in our system, the transmission coefficient measure is found to be $S_{21M} = (AS_{21})/(1 - \Gamma_o^2)$, where A is the attenuation factor. Therefore, the addition of an attenuator comes with a cost of reduction of the dynamic range of the measurement system. In our application and because of the high dynamic range of the amplitude and phase measurement system AD8302 (60 dB), this dynamic range reduction can be tolerated because our measurement specification is 25 dB. The addition of the transmission line segment $e^{-\gamma l}$ to this model is needed to understand the behavior of the system in the measurement phase and the unexpected error that has been introduced, such as a ripple in the transmission measurement when the input coaxial cable is long compared to the wavelength.

The Calibration Algorithm

The calibration algorithm that is used in this system is a normalized calibration or a self-calibration algorithm. The analysis of the vector network calibration in Bryant book [11] in section 2.11 reduces the problem of calibration into a five-elements network calibration problem. The designed system does not measure the reflection parameters, which reduces our system calibration standards from open, close, load, and thru into only Thru standards. Therefore, in order to calibrate our device, we need five measurements for five various lengths of a transmission line, which used as thru standards. The number of measurement can be reduced by applying the switched phase network in the system to add additional phase shift to the existing standard, which reduces our standards into only three different measurements. As our problem is of a special nature, and we need to concentrate on the resonant frequencies of the transmission line, a simpler calculation algorithm of normalization can be applied. In addition, the actual measurement of the material characterization is satisfactory and within reasonable error.

4.4 System Implementation

The software and hardware parts of the system have been highlighted and discussed in the following subsections. Some components of the system have been discussed, and their implementation methodologies have been described. The final physical system prototype of the phase amplitude meter is shown in Figure 4.4.

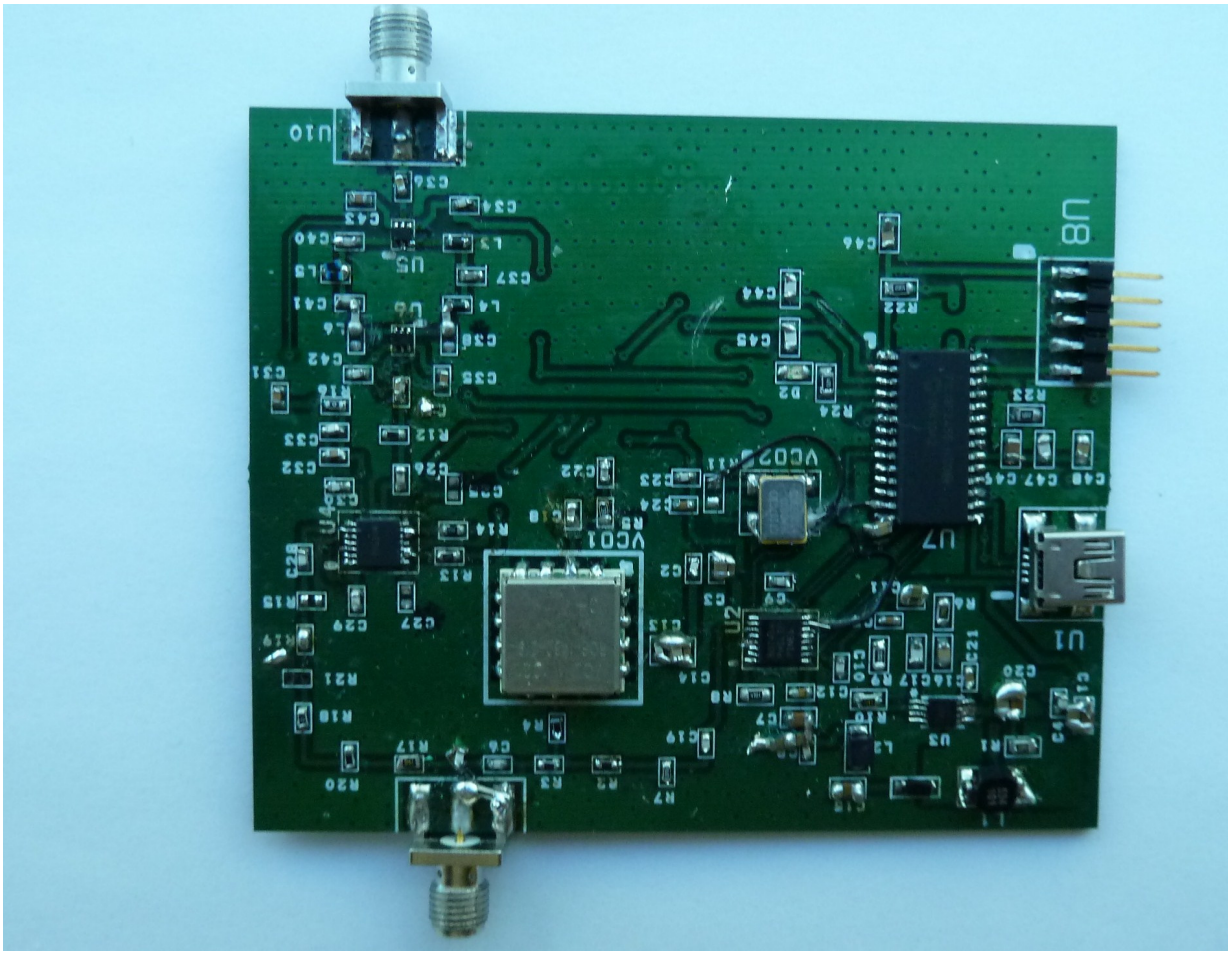

Figure 4.4: Assembled Printed Circuit Board (PCB) of the Transmission Meter

4.4.1 Hardware Implementation

This part discusses the implementation of the five main top level components mentioned in section 4.2. The detailed schematic of the system can be found in Appendix B.

μController

The μcontroller is from 18F family from Microchip^{TM}, specifically 18F2455[21]. This μcontroller has a built-in universal serial bus (USB) controller with a 3.3 V regulator for USB controller. Moreover, it has a 10 channels 10-bit analog to digital convert (ADC), which will be used to measure the phase and amplitude meter DC signals. The programming language for the 18F family is C, which speeds up the developments. The communi-

cation protocol between chips, Serial Peripheral Interface (SPI), is hardware implemented in this *mu*controller. This protocol is used to control the frequency synthesizer in the Oscillator subsystem. The control signal to the phase switched network is assigned to two general port input outputs (GPIOs).

Oscillator

The frequency generation in the transmission meter is generated by this subsystem. To cover the wide frequency range of the system, a Mini-Circuits® voltage control oscillator (VCO) (ROS-1480-219+) is used. This VCO [23] spans a range of the frequency 680 MHz up to 1480 MHz, which covers our range of interest. To achieve this wide range of operation, the control voltage of the VCO has to go up to 8.5 V. This high voltage was achieved in our 5 V system by introducing DC-DC boost converter. The reference frequency was done using a Voltage Controlled/Temperature Compensated Crystal Oscillator (VCTCXO) with frequency of 16 MHz, which also has been used as the main frequency of the μcontroller. For the demand of high voltage output for the control signal and the wide frequency range ADF4113HV synthesizer was chosen, as it satisfies these requirements [3]. The design of the loop filter of the VCO was done using ADIsimPLL™ simulation tool. The design of the switching power supply was done using ADISimPower™. The controlling of the Frequency synthesizer was done using SPI protocol controlled by the μController.

Amplitude and Phase Meter Subsystem

The core of this system is AD8302, which is an IF/RF Gain and Phase detector Integrated circuit(IC) from Analog Devices. This IC [2] has a 60 dB dynamic range and a wideband operation range (LF-2.7 GHz). The system detection architecture in this IC is direct detection.

Power Sampling and Isolator

The main functionality of the power sampling is to provide a reference path to the amplitude and phase detector subsystem. Due to the need of a low level coupler (Coupling of -30 dB) and the broadband of the coupled circuit, a simple resistive coupler has been used. Due to the coupling requirement, a low coupling loss can be achieved. The design of the power coupler tap is shown in 4.5. Agilent Advanced design System (ADS) software has been used to optimize the coupler; the coupling is -30 dB, and the insertion loss is -0.27 dB, and the worst return loss is -30 dB. The values of the resistances was found Rtap is 765.6 Ohm, and Rmatch is 53 Ohm.

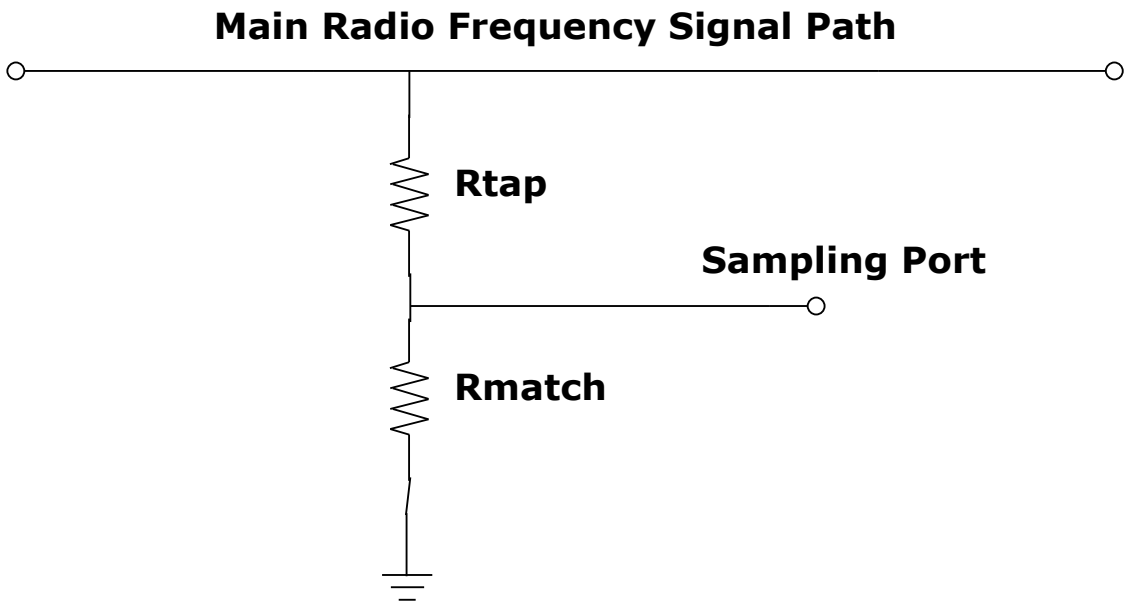

Figure 4.5: Power Sampling Circuit

The isolator is a simple 13 dB resistive attenuator. The large dynamic range of the amplitude and phase mater has allowed this compromise in the dynamic range, while achieving the overall system performance as per specifications. This implementation was used to optimize the isolator.

Other architectures for this set up has been investigated, mainly the "VSWR Bridge", which is based on balanced-unbalanced (BALUN) devices. This would get the appropriate low coupling and isolation with the addition of small a mount of loss. This solution has not been investigated further in this design meter, mainly to keep our objective of a simple and affordable measurement system.

Switched Phase Shifter

The switched phase shifter has been added due to the limitation of the AD8302. Specifically, in the phase measurement, there exists a phase sign ambiguity and a large error uncertainty up to 7° when the phase of the two input signals is in-phase [2]. The proposed solution is adapted from [37], where the author has used low-pass/high-pass (LP/HP)

lumped phase shifter architecture to measure a signal off-phase, which solves the problem of the accuracy. In addition, having two paths with a known phase shift, the phase ambiguity can be resolved.

The Agilent ADS was used to simulation and design of the phase shifter. The phase shifter is optimized to 40° phase shifting. There are two instances of the phase shifter simulations; the first one is using idealized components of the inductors and capacitors, shown in Figure 4.6. To gain more realistic results and check for any problems due to the self resonance of the inductors and the capacitors, an elaborate model has been used. The capacitors and inductors measured models were used from a library provided by Murata company, which is the inductors and capacitors manufacturer. This library provides a measurement of a sample of the actual components which makes our simulation more realistic. The values of the phase shifter are 1.8 nH and 1.5 pF for the Low pass branch and 39 nH and 30 pF for the High pass branch.

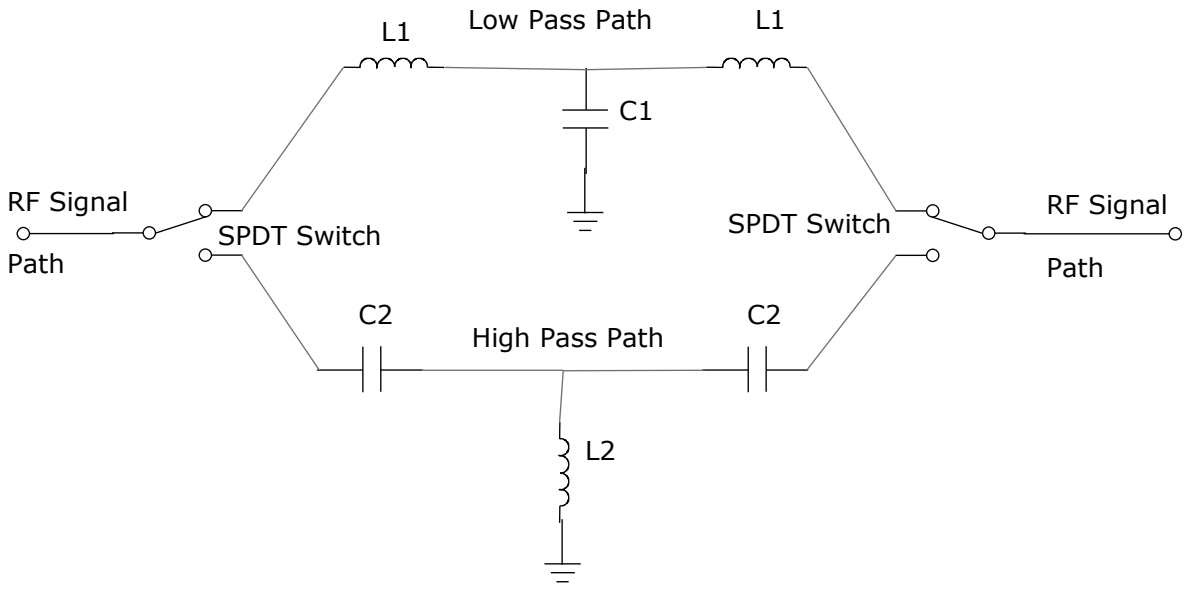

Figure 4.6: Switched Phase Shifter Network Using Ideal Components

As shown in Figure 4.7, both the ideal and the measurement library models have an agreement within our frequency of interest. Furthermore, the phase shift optimization is within ±5° of the nominal design phase shift. The deviation between the ideal and the realistic components has been observed for the high frequencies, that is mainly due to the self resonant frequency (SRF) of the components. In addition, the maximum insertion loss

of the phase shifter is -0.2 dB, and the worst return loss is 19 dB. These are within the band of interest.

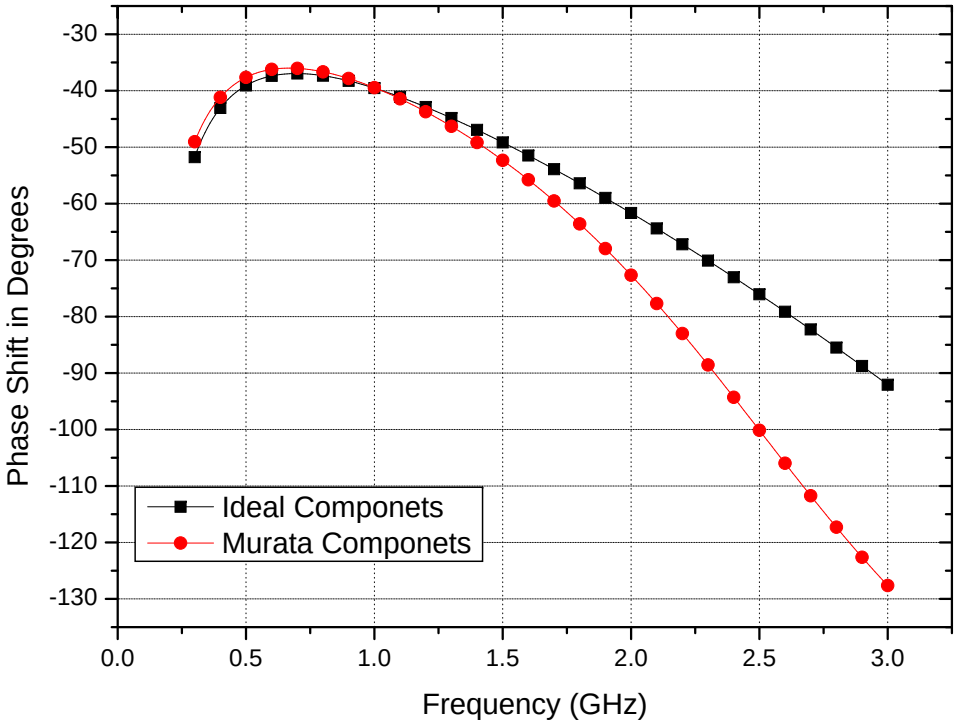

Figure 4.7: Phase Shifting Results Ideal versus Library Models

4.4.2 Embedded Software Development and Implementation

The software used in the PIC® *mu*controller device is programmed using the C programming language. This programming language was chosen because the productivity is higher than using an assembly programming language, and the resources and libraries implementation for 18F PIC family are easily available [18]. The complete C code is included in Appendix C.

The algorithm used in the implementation of the embedded software is described in the flow graph shown in Figure 4.8. This software architecture is using a simple infinite loop with interrupt service routines(ISRs). This implementation is adapted here instead of

the real time operating system (RTOS) because of its the simplicity and ease of programming [6].

The choice of the universal serial bus (USB) communication protocol is the communication device class (CDC)[18]. This was used to implement a virtual serial port communication protocol in order to simplify the programming of the desktop application on the PC side, as the serial port communication libraries are easily available for desktop applications[4]. In addition, this will simplify the debugging of the system in the early phases of the project development because an already available communication tool (HyperTerminal) is used to verify the hardware system.

The ISRs are used for the blinking the light emitting diode (LED) as an alive and debugging inductor. This was implemented as an low priority ISR to prevent the interruption of the other critical tasks.

As illustrated in Figure 4.8, the first step in the program is to initialize all the system parameters, specifically, USB, serial peripheral interface (SPI), and analog to digital converter (ADC) subsystems. The control of the frequency synthesizer uses the SPI protocol to set the proper frequency, then the phase and amplitude meter DC signals are measured using *mu*controller ADC, then the measured values and the channel number are sent the PC using the USB CDC protocol. The channel is looped over all the frequencies of interest. The phase path is toggled after the measured frequency range is covered.

4.5 Measurement Setup and Results

In this section, the measurement setup used will be discussed. Moreover, the bench mark sensor used for the analyzes of the applicability of this system will be discussed. The data will be analyzed and compared with the one collected from a vector network analyzer measurement, and the error percentage will be calculated to compare the system.

4.5.1 The Measurement Setup

The system setup is implemented to measure complementary split ring resonator (CSRR) sensor discussed and analyzed in the work of boybay's paper [9]. In this paper, the CSRR sensor for material characterization is suggested, analyzed, simulated, and implemented. The measurement for CSRR sensor uses a vector network analyzer (VNA), in order to extract the permittivity of the material under measurement (MUM). The minimum transmission coefficient(resonant) frequency of the CSRR has a proportional relation with permittivity of the MUM.

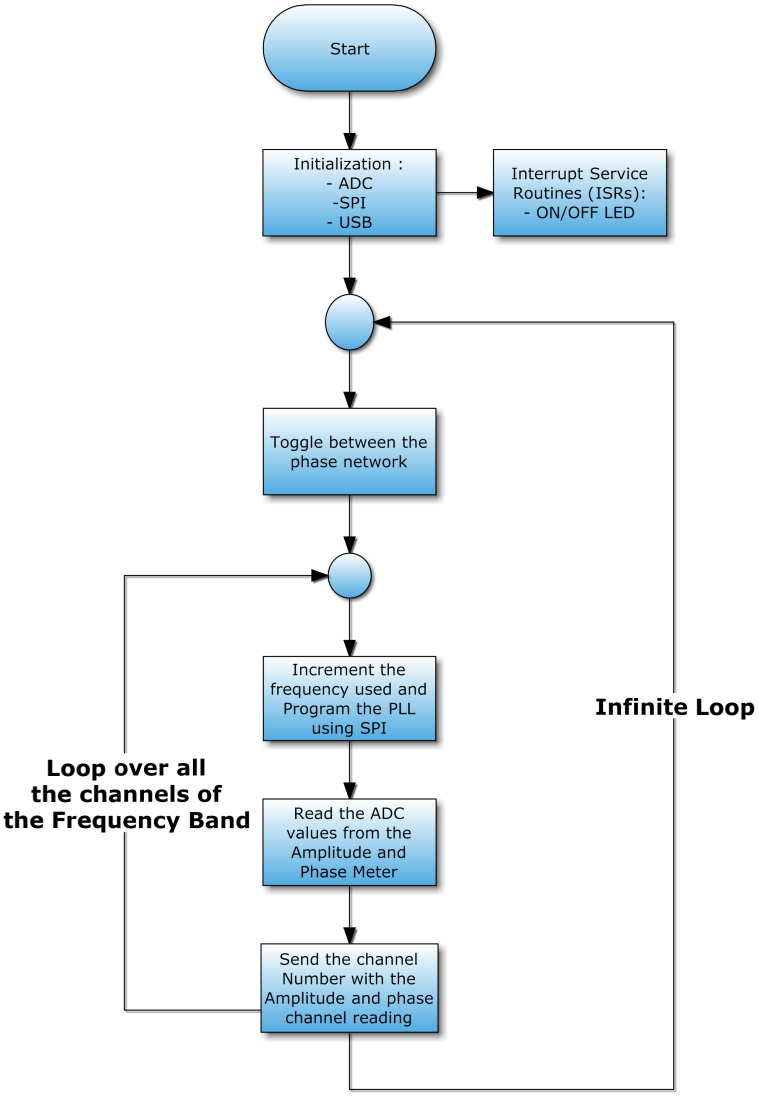

Figure 4.8: Algorithm Flow Graph of the Implemented Embedded Software

The measurement setup is shown Figure 4.9, where the device is connected to the sensor using two coaxial cables. The coaxial cables are kept as short as possible in order to reduce the measurement errors.

In order to characterize the materials, the MUM is stacked at the sensor as shown in Figure 4.10. The measurement of the transmission coefficient uses the transmission meter and using HyperTerminal in the PC to collect the measured data.

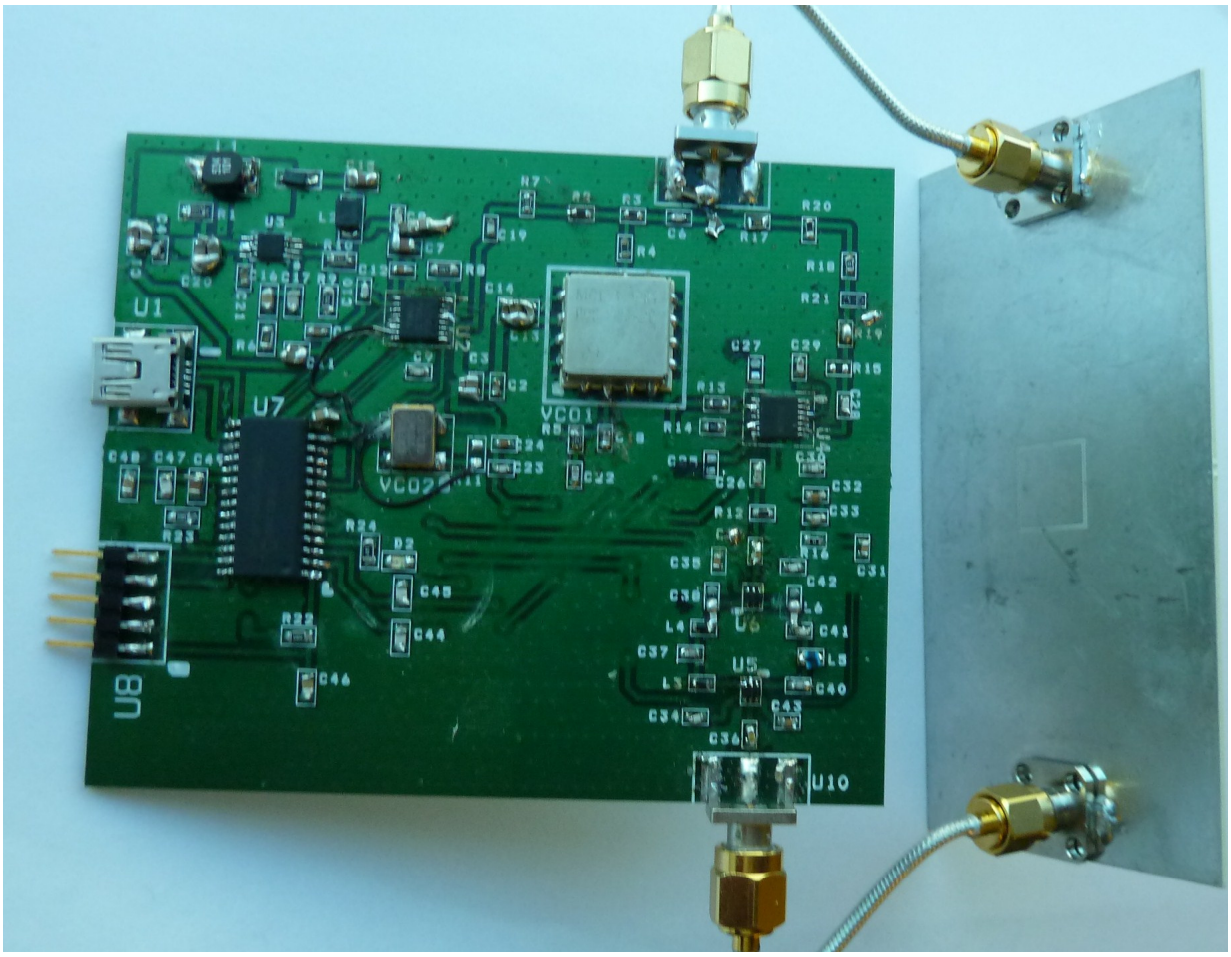

Figure 4.9: Transmission Meter with the Sensor

4.5.2 Experiment and Data Analysis

Four different dielectric materials are measured using the transmission system. The materials are Air, Roger 3003, Teflon, and FR-4, and the measurement results are shown in Figure 4.11 and their error percentages are summarized in Table . The permittivity extraction algorithm adapted in this work is a linear relationship between the resonant frequencies and the permittivity. This can be inferred on analysis of CSRR sensor [9]. In addition, two reference materials (permittivity calibration standards) are used to find the linear relationship to be used in the extraction algorithm.

In experiment set up, Air and FR-4 are used as calibration standards. The other two materials are considered as test materials to compare the accuracy of our system with their known permittivity. The results are summarized in table 4.2. As can be seen from table,

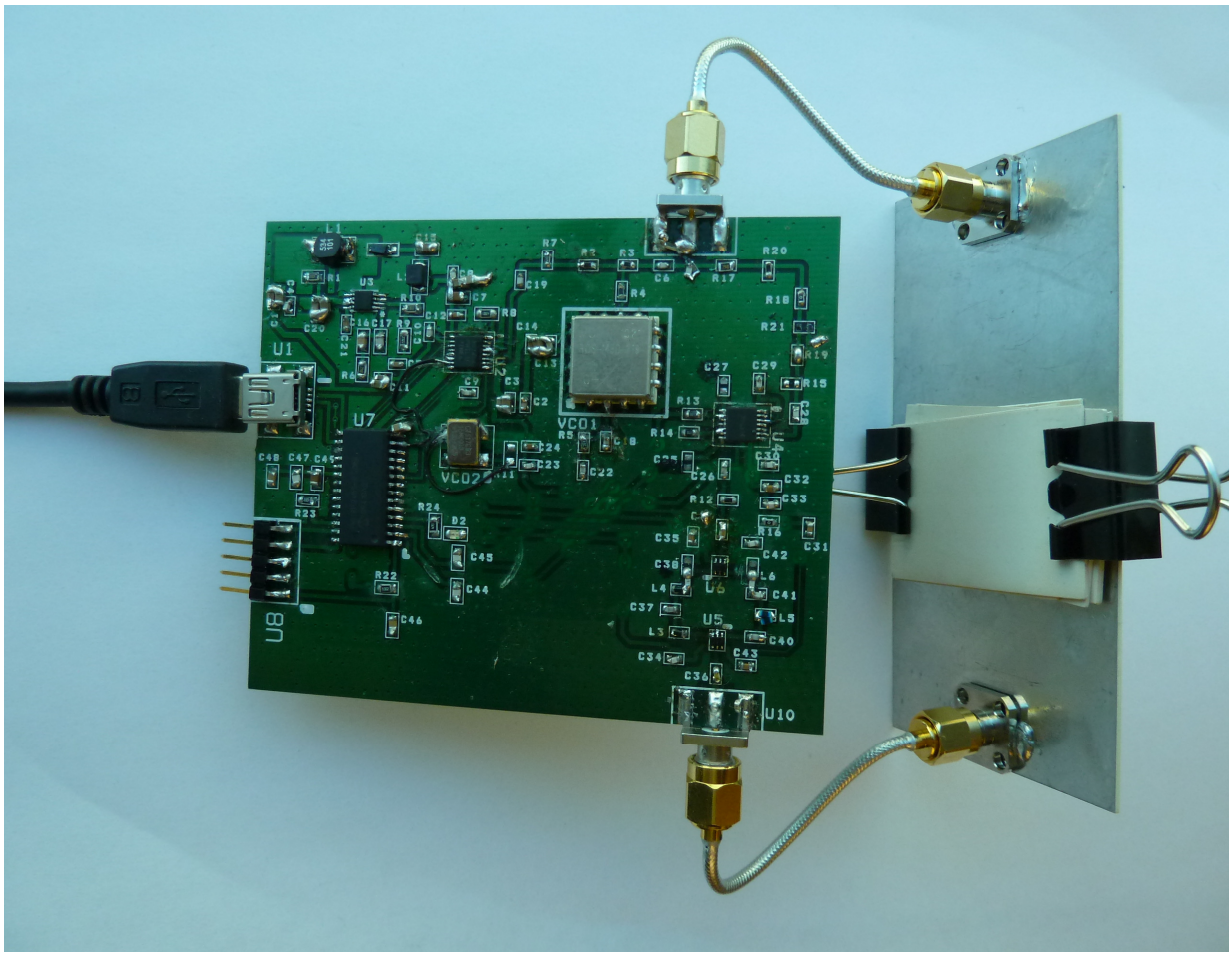

Figure 4.10: Transmission Meter with Material Under Measurement (MUM) and the Sensor

the maximum error of the extracted value is 2.3%, which is a very good agreement with the material permittivity.

4.6 Conclusion

In this chapter, the design of the transmission meter has been investigated and the design methodology of its main subsystems has been discussed. System level analysis and main sources of the errors and methodologies to reduce it has been discussed. In addition, a full schematic and code have been included in the appendix B and C for further investigation for whom is interested.

To validate our design, the transmission measured system is used to characterize ma-

Material Name	ϵ_r	$f@S_{21}min$ using VNA (MHz)	$f@S_{21}min$ using Transmission Meter (MHz)	Error Percentage (%)
FR-4	4.3	967	959	-0.8
RO 3003	3	1053	1044	-0.9
Teflon	2.1	1097	1095	-0.2
Air	1	1160	1164	0.3

Table 4.1: Comparison of the Frequencies at the Minimum Transmission Coefficient Between the Transmission Meter and the VNA

Material Name	ϵ_r	$f@S_{21}min$ using Transmission Meter (MHz)	Extracted ϵ_r	Error Percentage (%)
FR-4	4.3	959	Used As Calibration Standard	-
Air	1	1164	Used As Calibration Standard	-
RO 3003	3	1044	2.93	-2.3
Teflon	2.1	1095	2.11	0.5

Table 4.2: Results of the Transmission Meter used to Calculate Permittivity of Different Materials and the Measurement Error Percentages

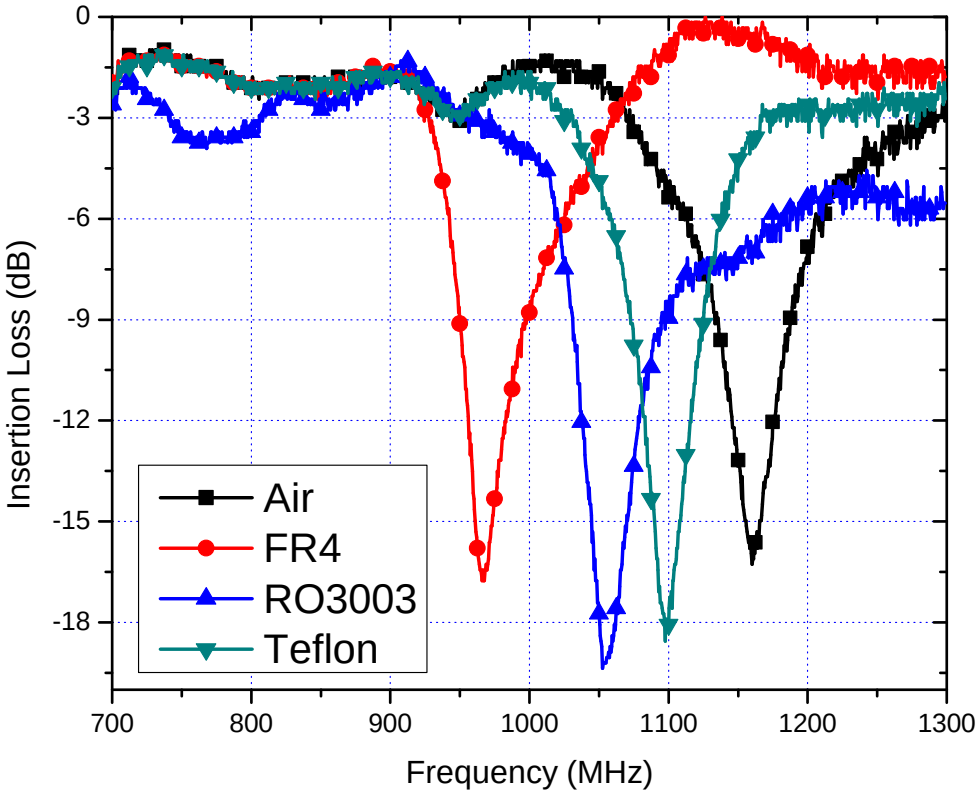

Figure 4.11: Transmission Meter S_{21} Measurements

terials' permittivity. A comparison between a vector network analyzer (VNA) and this system measured data using the complementary split ring resonator (CSRR) sensor has been shown in table 4.1. The results shows an agreement with the VNA reference results, which is concluded by the low error percentage in data measured. A test case setup uses a linear permittivity extraction algorithm for CSRR showed a practical application for our system. The maximum error of the material permittivity measurement is 2.3%. The prototype cost did not exceed 100 CAD. This cost includes the Bill of Material (BOM) and printed circuit board (PCB) prototype cost, which is an affordable solution for industrial applications such as food manufacturing process controller.

Chapter 5

Conclusion and Future Work

5.1 Conclusion

In this work, the utility of using an RF direct detection circuits for the application of material characterization and crack detection in conjunction with metamaterial probes is investigated. Two measurement prototypes have been designed and implemented. One prototype is to measure the phase variation of the reflection coefficient due to the presence of a small crack in a conducting sheet. The second prototype is to measure the transmission coefficient for material characterization applications. Both these prototypes have been tested and the results compared with the results obtained from a vector network analyzer measurement. The results show strong agreement.

In this work, the final metamaterial-based sensor system demonstrated the possibility of designing a highly accurate, compact, lightweight, and inexpensive system operating in the low GHz frequency regime. The system can be designed for higher frequencies to achieve higher lateral detection resolution or higher material detection sensitivity, however, at the cost of increasing components cost and deterioration in depth resolution.

5.2 Future Work and Enhancement

In the phase meter prototype device (chapter 3), additional enhancements is required to reach an optimum solution for crack detection. These enhancements include the following:

- Substitution of the DAQ card and the computer with a μcontroller and embedded user interface to give a more realistic independent and compact solution.

- Employing a frequency synthesizer to set the frequency instead of a potentiometer to increase the accuracy and eliminate the need for re-calibration of the potentiometer every-time you need to start the measurement process.
- Use of a multi-path phase shifter before the sensor by introducing a switched phase shifter such as the one implemented in the transmission meter (chapter 4). This addition will extend the phase range of the phase measurement and enable an automatic calibration of the system.

For the transmission meter (Chapter 4), the following future works are suggested:

- Addition of an embedded input and output user interfaces, which will give the proper results of the measurement of permittivity. This will eliminate the use of a computer and will make the sensor more portable.
- Extension of the extraction algorithm in order to detect the moisture content in the material, mainly, seeds or grains. This enhancement will address the main motivation for this work, which is the usage of this technology in the in-farm storage bins.
- Elimination of the AD8302 detector integrated circuit. This IC provides an excellent detection for amplitude and phase with a high accuracy. However, this performance comes with a price which increases the cost of the system. The system does not require very high dynamic range, thus, a simpler design can be adopted for phase and amplitude detection.

In addition, a general future work for the whole project in order to achieve a compact, lightweight, affordable, and accurate meter would be as follows:

- Extension of the material characterization algorithm to be used to measure moisture. This extraction algorithm can utilize the phase reading and amplitude to extract the phase variation and amplitude attenuation.
- Integration of the sensor in the PCB. The sensors used in the system are all planar and adapt themselves into PCB integrations, and this will enable a more compact sensor.
- Further system testing with other metamaterial sensors in addition to theoretical work on the metamaterial sensor design. There are some challenges that need to be addressed in the metamaterial sensor, such as loss and extraction algorithms for material characterization.

References

[1] M.A. Abou-Khousa, M.A. Baumgartner, S. Kharkovsky, and R. Zoughi. Novel and simple high-frequency single-port vector network analyzer. *Instrumentation and Measurement, IEEE Transactions on*, 59(3):534 –542, 2010. 1, 11

[2] Analog Devices Inc. RF/IF Gain and Phase Detector AD8302 DataSheet, 7 2002. 24, 30, 31

[3] Analog Devices Inc. High Voltage Charge Pump, PLL Synthesizer ADF4113HV DataSheet, 9 2008. 30

[4] J. Axelson. *USB complete: everything you need to develop custom USB peripherals*. lakeview research llc, 2005. 34

[5] J. Baker-Jarvis, M. D. Janezic, J. H. Jr Grosvenor, and R. G. Geyer. Transmission/reflection and short-circuit line methods for measuring permittivity and permeability. Technical Report NIST/TN 1355, May 1992. 6

[6] Michael Barr, Anthony J. Massa, 1971-Programming embedded systems in C Barr, Michael, and C++. *Programming embedded systems : with C and GNU development tools*. O'Reilly, Beijing ; Cambridge, 2006. 34

[7] M.S. Boybay and O.M. Ramahi. Near-field probes using double and single negative media. *Physical Review E*, 79(1):16602, 2009. 2, 5, 6, 9

[8] M.S. Boybay and O.M. Ramahi. Waveguide Probes Using Single Negative Media. *Microwave and Wireless Components Letters, IEEE*, 19(10):641 –643, 2009. 9

[9] Muhammed S. Boybay and Omar M. Ramahi. Material characterization using split-ring resonators. To be published. 2, 5, 8, 24, 34, 36

[10] J.R. Brence and D.E. Brown. Quantifiable Corrosion Detection in Aging Aircraft. Technical Report SIE-060001, University of virginia, 2006. 1, 2

[11] G. H. Bryant. *Principles of Microwave Measurements*. Peter Peregrinus Ltd., 1988. 14, 18, 25, 26, 28, 47

[12] L. Chen and V.K. Varadan. *Microwave electronics: measurement and materials characterization*. John Wiley & Sons Inc, 2004. 6

[13] M.A. El Sabbagh, O.M. Ramahi, S. Trabelsi, S.O. Nelson, and L. Khan. Use of microstrip patch antennas in grain and pulverized materials permittivity measurement. In *Antennas and Propagation Society International Symposium, 2003. IEEE*, volume 4, pages 42 – 45 vol.4, 2003. 1, 3, 11

[14] G.F. Engen. The Six-Port Reflectometer: An Alternative Network Analyzer. *Microwave Theory and Techniques, IEEE Transactions on*, 25(12):1075 – 1080, December 1977. 10

[15] F.M. Ghannouchi and R.G. Bosisio. Measurement of microwave permittivity using a six-port reflectometer with an open-ended coaxial line. *Instrumentation and Measurement, IEEE Transactions on*, 38(2):505 –508, April 1989. 1, 10

[16] F.M. Ghannouchi and A. Mohammadi. *The six-port technique with microwave and wireless applications*. Artech House Publishers, 2009. 10

[17] Q. Gu. *RF system design of transceivers for wireless communications*. Springer Verlag, 2005. 10

[18] Dogan Ibrahim. *Advanced PIC microcontroller projects in C : from USB to ZIGBEE with the 18F series*. Newnes/Elsevier, Amsterdam ; Boston, 2008. 33, 34

[19] RJ King. Microwave homodyne systems. 1978. 10

[20] Zhaowei Liu, Nicholas Fang, Ta-Jen Yen, and Xiang Zhang. Rapid growth of evanescent wave by a silver superlens. *Applied Physics Letters*, 83(25):5184 –5186, December 2003. 8

[21] Microchip Technology Inc. PIC18F2455/2550/4455/4550 Data Sheet: 28/40/44-pin, High-Performance,Enhanced Flash, USB Microcontrollers with nanoWatt Technology, 10 2009. 29

[22] Mini-Circuits. Surface Mount Micro-Miniature Power Splitter/Combiners SBTC-2-15-75+/SBTC-2-15-75L+ DataSheet, 2010. 18

[23] Mini-Circuits. Surface MountVoltage Controlled Oscillator ROS-1480-219+ DataSheet, 2010. 30

[24] S. Neethirajan and D. S. Jayas. Sensors for Grain Storage. In *ASABE Annual International Meeting, Technical Papers*, volume 12. American Society of Agricultural and Biological Engineers, 01 2007. NR: 28; RP: 076179; NU: 350036441. 1, 3

[25] S. Neethirajan, C. Karunakaran, D.S. Jayas, and N.D.G. White. Detection techniques for stored-product insects in grain. *Food Control*, 18(2):157 – 162, 2007. 2

[26] Seichi Okamura, Yangjun Zhang, and Nobuhito Tsukamoto. A new microstripline-type moisture sensor for heavily wet tea leaves. *Measurement Science and Technology*, 18(4):1022, 2007. 1, 11

[27] Brabec-D.L. Schwartz C.R. Pearson, T.C. Automated detection of internal insect infestations in whole wheat kernels using a perten SKCS 4100. *Applied Engineering in Agriculture*, 19(6):727–733, 2003. cited By (since 1996) 14. 3

[28] J.B. Pendry. Negative refraction makes a perfect lens. *Physical Review Letters*, 85(18):3966–3969, 2000. 5, 6, 8, 9, 11

[29] D.M. Pozar. Microwave Engineering, 3rd, 2005. 9

[30] B. Razavi. Design Considerations for Direct-Conversion Receivers. *Circuits and Systems II: Analog and Digital Signal Processing, IEEE Transactions on*, 44(6):428 –435, June 1997. 10

[31] B. Razavi and R. Behzad. *RF microelectronics*, volume 225. Prentice Hall Upper Saddle River, NJ, 1998. 10

[32] Zhao Ren, M.S. Boybay, and O.M. Ramahi. Near-field subsurface detection in lossy media using single split resonator probe. In *Wireless Sensing, Local Positioning, and RFID, 2009. IMWS 2009. IEEE MTT-S International Microwave Workshop on*, pages 1 –3, 2009. 2, 21, 22

[33] Zhao Ren, M.S. Boybay, and O.M. Ramahi. Metamaterial inspired probe for noninvasive near-field subsurface sensing. In *Antennas and Propagation Society International Symposium (APSURSI), 2010 IEEE*, pages 1–4, 2010. 5, 14, 19

[34] DR Smith, W.J. Padilla, DC Vier, S.C. Nemat-Nasser, and S. Schultz. Composite medium with simultaneously negative permeability and permittivity. *Physical Review Letters*, 84(18):4184–4187, 2000. 6, 8

[35] N.N. Suwan, M.S. Boybay, and O.M. Ramahi. ENG-Sensor: Enhanced open-ended coaxial line sensor for material characterization application. In *Antennas and Propagation Society International Symposium (APSURSI), 2010 IEEE*, pages 1–4. IEEE, 2010. 2, 8, 9

[36] K Vijayakumar, S R Wylie, J D Cullen, C C Wright, and A I Ai-Shamma'a. Non invasive rail track detection system using microwave sensor. *Journal of Physics: Conference Series*, 178(1):012033, 2009. 1

[37] Sam Wetterlin. Use Of Phase Shift to Resolve Sign Ambiguity and Improve Accuracy in The AD8302 Phase Detector, 3 2007. 31

[38] A. Yariv and P. Yeh. *Photonics: Optical Electronics in Modern Communications (The Oxford Series in Electrical and Computer Engineering)*. Oxford University Press, Inc. New York, NY, USA, 2006. 9

[39] L. Yousefi, M.S. Boybay, and O.M. Ramahi. Experimental retrieval of the effective parameters of metamaterials using a strip line method. In *Antennas and Propagation Society International Symposium (APSURSI), 2010 IEEE*, pages 1 –4, 2010. 6

[40] Joseph N. Zalameda, Robert F. Anastasi, and Eric I. Madaras. Nondestructive evaluation (nde) results on sikorsky aircraft survivable affordable. 2004. 1, 2

APPENDICES

Appendix A

Error Equation Derivation

In this appendix we derive equation 4.1 for error analysis for the transmission meter device. The analysis follows closely the analysis done in Bryant book [11], which is based on the Non-touching loop rule (mason's rule):

$$T = \frac{\sum_K T_K \Delta_K}{\Delta} \tag{A.1}$$

where

T_K : path gain on the Kth forward path between the nodes

Δ : $1 -$ (sum of all individual loop gains)
+(sum of loops gain products of all possible
combinations of two non-touching loops)
−(sum of loops gain products of all possible
combinations of three non-touching loops)
...

Δ_K : sum of all terms in Δ not touching the kth path

From Figure 4.2 and noting that the individual loop gains is $e^{-\gamma l}\text{Iso}\Gamma_{PT}\Gamma_{Mckt}$ and noting the path gain is $Le^{-\gamma l}$, the transfer equation is calculated by using mason's rule as follows:

$$\left.\frac{\text{OUT}}{\text{IN}}\right|_{withoutDUT} = \frac{Le^{-\gamma l}}{1 - e^{-\gamma l}\text{Iso}\Gamma_{PT}\Gamma_{Mckt}} \tag{A.2}$$

From Figure 4.3, the individual loop gains are $e^{-\gamma l}\text{Iso}\Gamma_{PT}\Gamma_{DUTin}$, $e^{-\gamma l}S_{21}\Gamma_{PT}S_{12}\Gamma_{DUTin}\text{Iso}\Gamma Mckt$, and $\Gamma_{DUTin}\Gamma Mckt$. In addition, the two non-touching loop

is
$e^{-\gamma l}\mathrm{Iso}\Gamma_{PT}\Gamma_{DUTin}e^{-\gamma l}S_{21}\Gamma_{PT}S_{12}\Gamma_{DUTin}\mathrm{Iso}\Gamma Mckt$, and the loop gain is $Le^{-\gamma l}S_{21}$ By applying the mason's rule the transfer function becomes as follows:

$$\left.\frac{\mathrm{OUT}}{\mathrm{IN}}\right|_{DUT} = \frac{Le^{-\gamma l}S_{21}}{1 - K\Gamma_{PT}\Gamma_{DUTin} - KS_{21}\Gamma_{PT}S_{12}\Gamma_o^2 - \Gamma_o^2 + K\Gamma_{PT}^2\Gamma_{DUTin}e^{-\gamma l}S_{21}S_{12}\Gamma_o^2} \tag{A.3}$$

where $K = \mathrm{Iso}e^{-\gamma l}$ and $\Gamma_o^2 = \Gamma_{DUTin}\Gamma_{Mckt}$

In order to get the measured value we need to self-calibrated (the loss and phase shift due to the original path are measured and canceled), to get the resulting measured transmission coefficient (S_{21M}), dividing equation A.3 by equation A.2 , the results are as follows:

$$S_{21M} = \frac{S_{21}(1 - K\Gamma_{PT}\Gamma_{Mckt})}{1 - K\Gamma_{PT}\Gamma_{DUTin} - KS_{21}\Gamma_{PT}S_{12}\Gamma_o^2 - \Gamma_o^2 + K\Gamma_{PT}^2\Gamma_{DUTin}e^{-\gamma l}S_{21}S_{12}\Gamma_o^2} \tag{A.4}$$

where $K = \mathrm{Iso}e^{-\gamma l}$ and $\Gamma_o^2 = \Gamma_{DUTin}\Gamma_{Mckt}$

Appendix B

Transmission Meter Schematic

In this appendix the schematics of the Transmission Meter design are included:

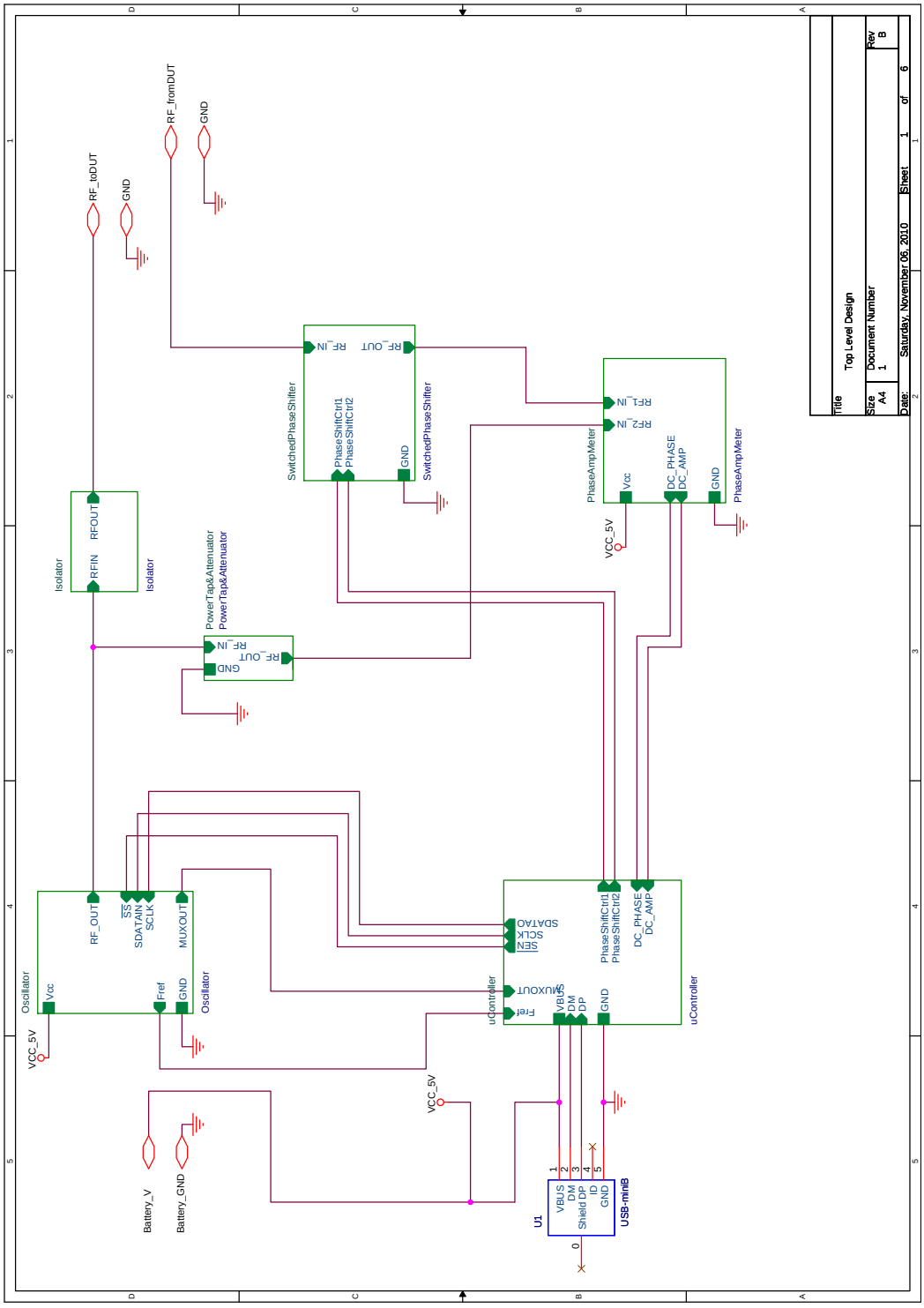

Figure B.1: Top Level Block Schematic

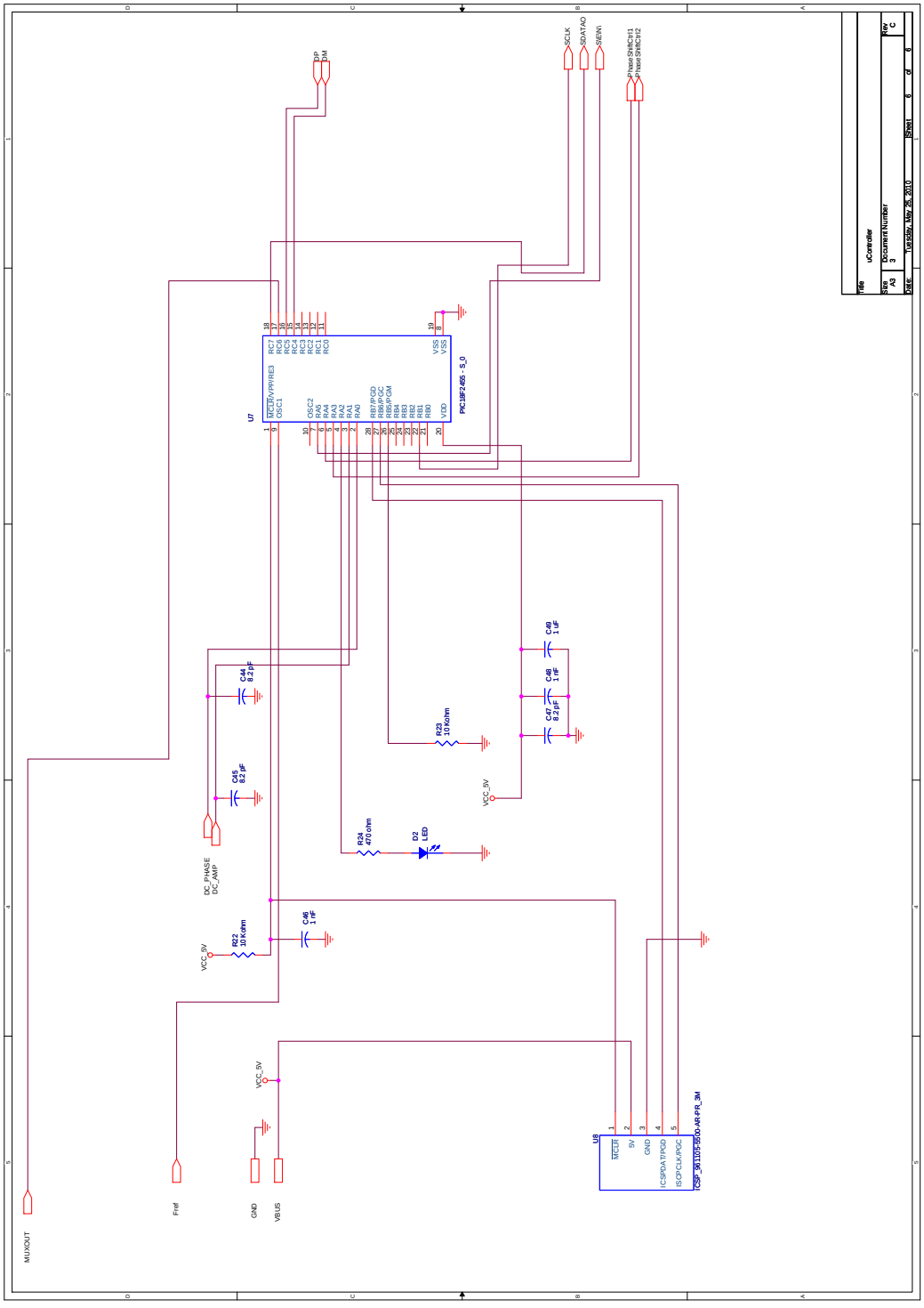

Figure B.2: μController Schematic

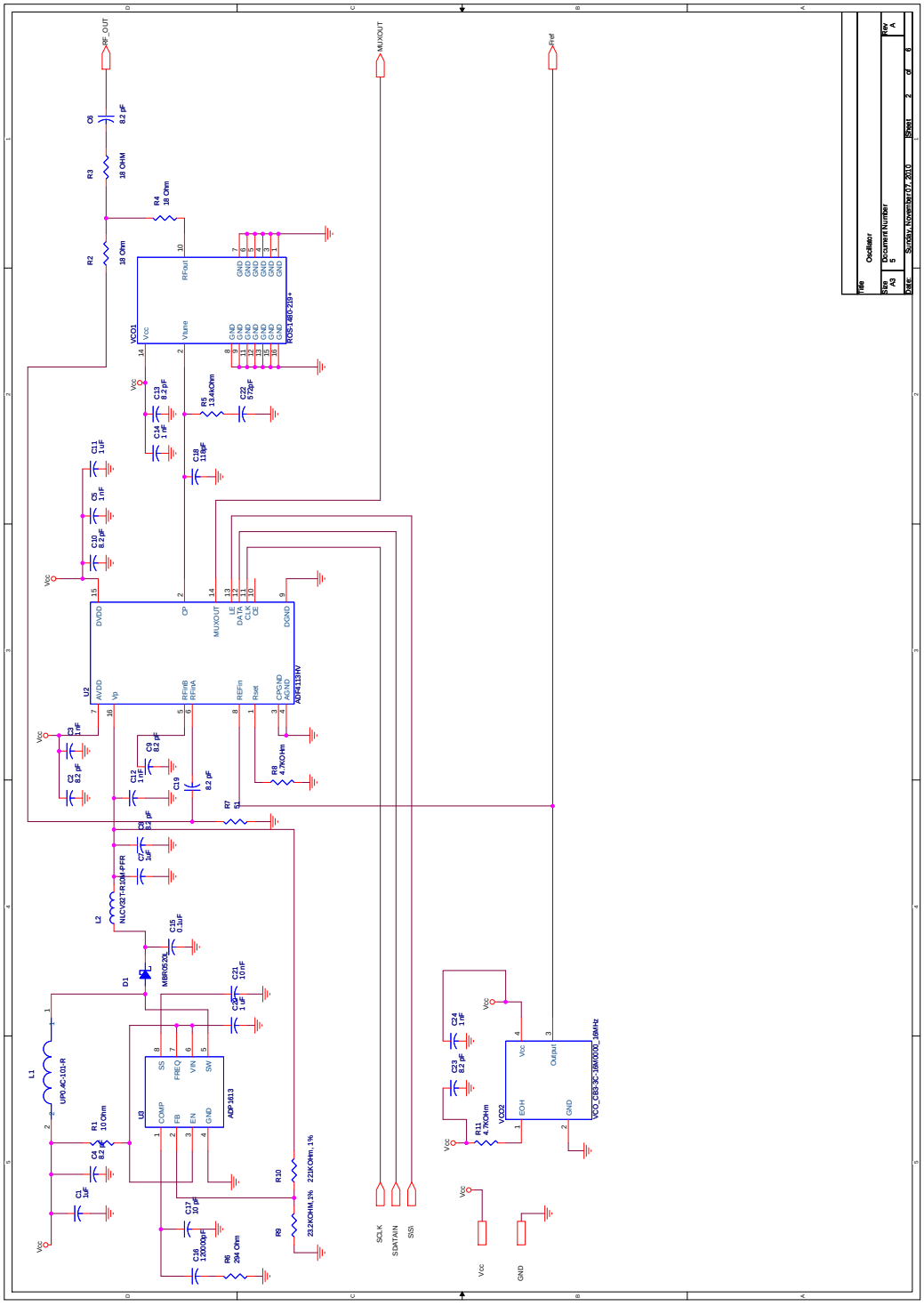

Figure B.3: Oscillator Schematic

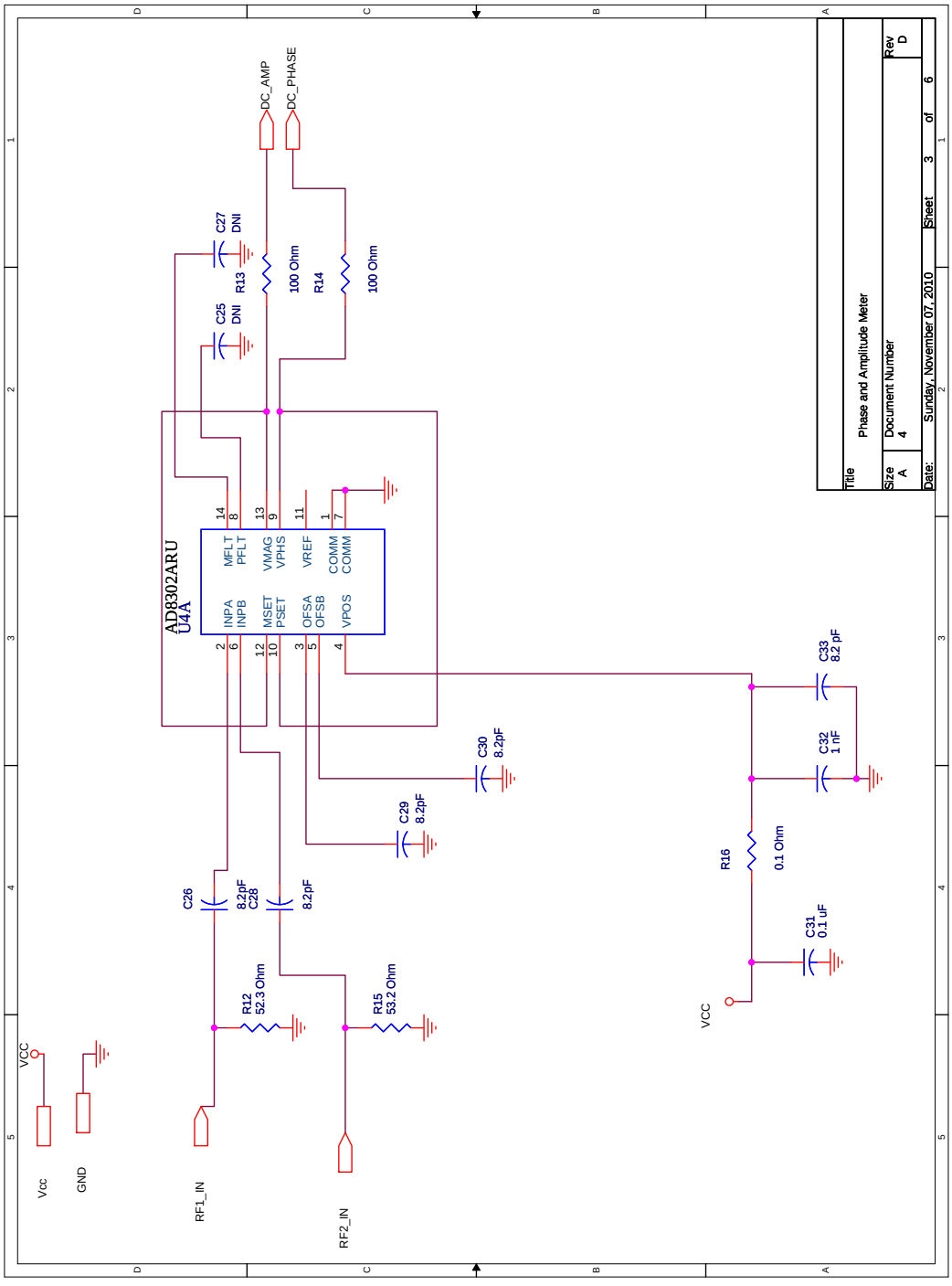

Figure B.4: Amplitude and Phase Meter Schematic

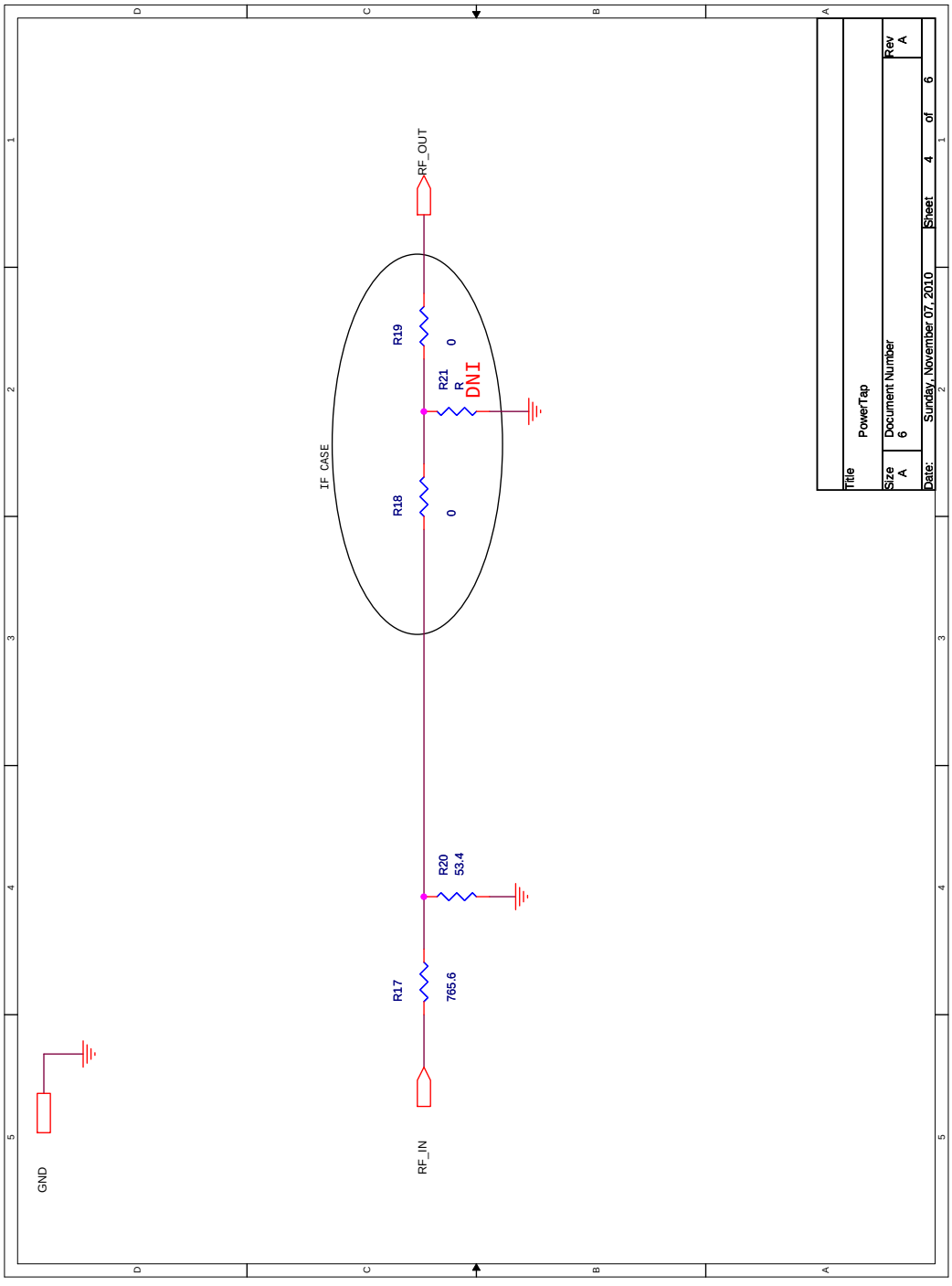

Figure B.5: Power Coupling Schematic

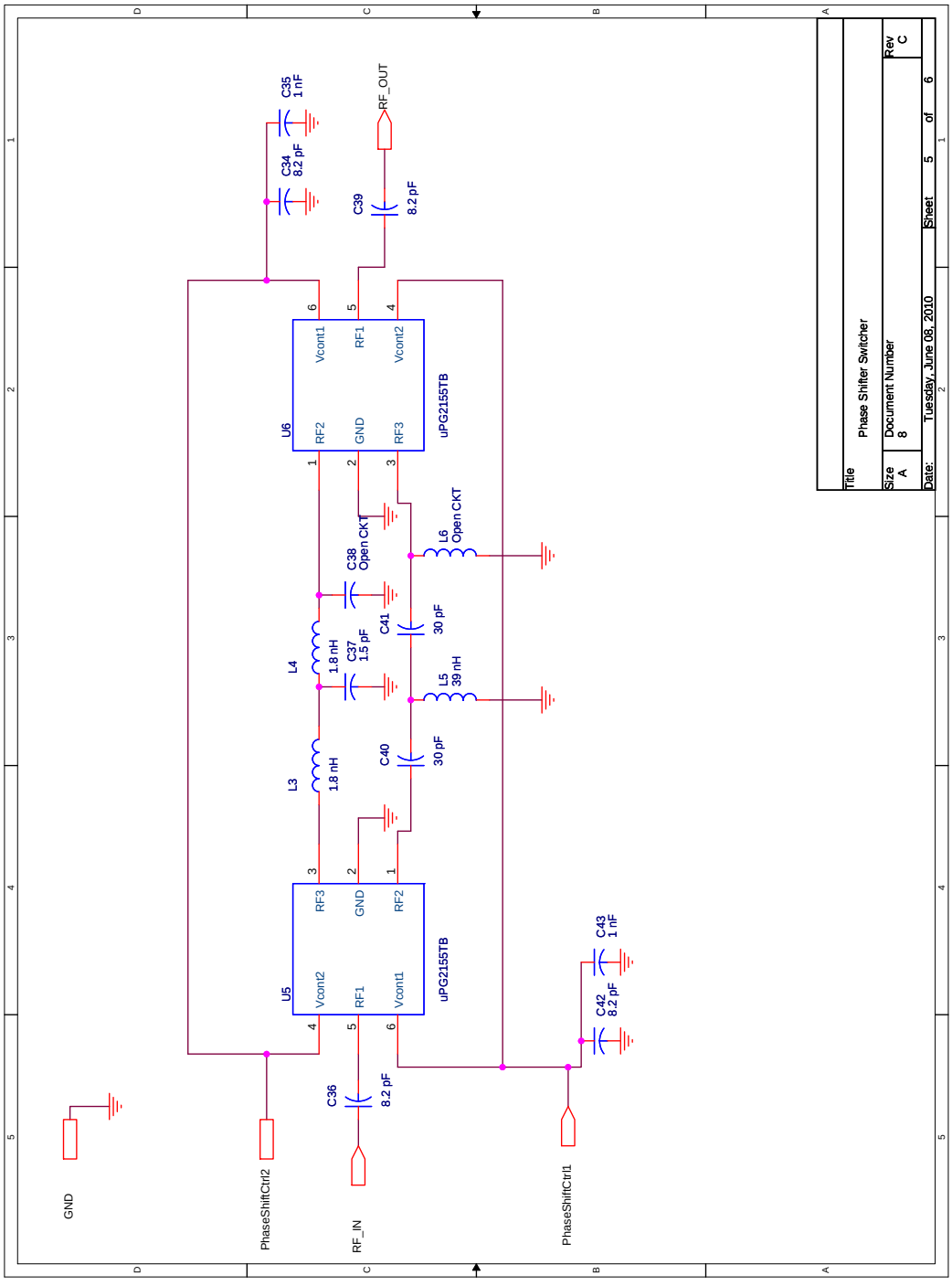

Figure B.6: Switched Phase Shifter Schematic

Appendix C

μController Code

```
#include <stdlib.h>
#include <usb_cdc.h>
#include "main_v9.h"



//this function will receive the three registers and
// then send the spi, the first is the MSBit and the
// last one of the third element is the LSBit
void write_spi_pll(char  FunctionLatch[3], char  RLatch[3],
char  NCounterLatch[3]);
//this function blinks every 500 ms
void IAmAlive();

#INT_TIMER0
void clock_isr(void)
{
  IAmAlive();
}

//adc read
void readADC(long* PtrAMPadcResult, long* PtrPMadcResult);


void main()
```

```
{
   //variable definations
   //the PLL Setting These are the default unless otherwise
   // modified later. the function latch setting
   //1 - 00 : 8/9
   //2 - 0000 : reserved !
   //3 - 000 : 80~uA for the 4.7~KOhm
   //4 - 000000 :reserved !
   //5 - 0 : the charge pump state is normal
   //6 - 1 : phase detector is normal state
   //7 - 001 :  digital lock detects
   //8 - 0 : power down normal
   //9 - 0 : counter reset, normal
   //10 - 10 : the address of this register.
   char FunctionLatch[3] = { 0b00000000, 0b00000000, 0b10010010};

   char NCounterLatch[3] = { 0b00000000, 0b10101111, 0b00000001};
   //R counter is set to
   char RLatch [3]       = { 0b00000010, 0b00000000, 0b10000000};
   long AMPadcResult;
   long PMadcResult;
   int i;
   char string[5];
   long counter = 0;
   long const NumberOfpoints =  1201;
   //these values corespond to 700~MHz
   long PLLA = 0;
   long PLLAshifted;
   long PLLB = 175;
   long PLLBshifted;

   setup_adc(ADC_CLOCK_DIV_64);
   setup_adc_ports(AN0_TO_AN1|VSS_VDD);
   setup_wdt(WDT_OFF);
   setup_timer_0(RTCC_INTERNAL|RTCC_DIV_128);
   setup_timer_1(T1_DISABLED);
   setup_timer_2(T2_DISABLED,0,1);
   setup_timer_3(T3_DISABLED|T3_DIV_BY_1);
   setup_comparator(NC_NC_NC_NC);
   setup_vref(FALSE);
```

```
   set_timer0(0);
   enable_interrupts(INT_TIMER0);
   enable_interrupts(GLOBAL);
   //Setup_Oscillator parameter not selected
   //from Internal Oscillator Config tab

    // TODO: USER CODE!!
    usb_init();

//  );
//  );

 #use SPI( DO=PIN_B1,    CLK=PIN_C7,    baud = 100000,    BITS = 8,
 MSB_FIRST,    SAMPLE_RISE,     stream = SPI_PORT0 )
    write_spi_pll(FunctionLatch, RLatch, NCounterLatch);


    output_high(PIN_A4);
    output_low(PIN_A3);
    delay_ms(5000);
    while(1)
    {
     //enable the shifter pin 1 ;
     //set_tris_a(0b11100111);
     //output_toggle(PIN_A4);
     //output_toggle(PIN_A3);
     delay_ms(10);
     PLLA = PLLA + 1;
     //write the registers to the PLL with modulus
     //equal to there max value.
     //reset to the intial values when reach 1300~MHz
     if( PLLA >= 0  && PLLB == 325)
     {
        PLLA = 0;
        PLLB = 175;
        //switch the phase shifter to the another path
        output_toggle(PIN_A4);
        output_toggle(PIN_A3);
        delay_ms(20);
        usb_cdc_putc('\n');
```

```
    usb_cdc_putc('\n');
    usb_cdc_putc('\n');
    usb_cdc_putc('\n');
    usb_cdc_putc('\n');
    usb_cdc_putc('\n');
}

//increament PLLB when PLLA overflow at PLLA = 16
if(PLLA == 8)
{
    PLLA = 0;
    PLLB++;
}

//reset PLLA
NCounterLatch [2] = (char)(NCounterLatch[2] & 0b00000011) ;

//shift PLLA two bits
PLLAshifted = PLLA << 2;

//assign the new values
NCounterLatch [2] = (char)(NCounterLatch[2]|PLLAshifted);

//assign lower PLLB
NCounterLatch [1] = (char)(PLLB & 0x000000FF);

//reset the upper PLLB
NCounterLatch [0] = (char)(NCounterLatch[0] & 0b11100000) ;

//shift PLL to the right by one byte
PLLBshifted = PLLB >> 8;
NCounterLatch [0] = (char)(PLLBshifted| NCounterLatch [0] );



// write the new PLL
write_spi_pll(FunctionLatch, RLatch, NCounterLatch);
delay_us(5000);
//write_spi_pll(FunctionLatch, RLatch, NCounterLatch);
//delay_ms(10);
```

```
//read the adc value
AMPadcResult = 255;
PMadcResult = 10;

//read the phase and amplitude reading
readADC(AMPadcResult,PMadcResult);

//send ADC using USB
itoa(counter, 10,string);
for ( i = 0; i < 5 ; i++)
{

     usb_cdc_putc(string[i]);
     string[i] = null;
}
usb_cdc_putc(',');

itoa(PLLA, 10,string);
for ( i = 0; i < 5 ; i++)
{
     usb_cdc_putc(string[i]);
     string[i] = null;
}
usb_cdc_putc(',');

itoa(PLLB, 10,string);
for ( i = 0; i < 5 ; i++)
{
     usb_cdc_putc(string[i]);
     string[i] = null;
}
usb_cdc_putc(',');

itoa(AMPadcResult, 10,string);
for ( i = 0; i < 5 ; i++)
{
     usb_cdc_putc(string[i]);
     string[i] = null;
}
```

```
      usb_cdc_putc(',');

      itoa(PMadcResult, 10,string);
      for ( i = 0; i < 5 ; i++)
      {
            usb_cdc_putc(string[i]);
            string[i] = null;
      }
      usb_cdc_putc(';');
      usb_cdc_putc('\n');

      counter = (counter + 1)%NumberOfpoints;
   }

}

void write_spi_pll(char FunctionLatch[3], char RLatch[3],
char NCounterLatch[3] )
{

  //disble the PLL
  output_low(PIN_C2);
  delay_cycles(3);
  set_tris_c(0b11111011);


  //write the function register
  spi_xfer(SPI_PORT0,FunctionLatch[0]);
          delay_cycles(3);
  spi_xfer(SPI_PORT0,FunctionLatch[1]);
          delay_cycles(3);
  spi_xfer(SPI_PORT0,FunctionLatch[2]);
          delay_cycles(3);
  set_tris_a(0b11101111);
  output_high(PIN_A5);
  delay_cycles(10);
  output_low(PIN_A5);

  //write the RLatch
  spi_xfer(SPI_PORT0,RLatch[0]);
```

```
        delay_cycles(3);
  spi_xfer(SPI_PORT0,RLatch[1]);
        delay_cycles(3);
  spi_xfer(SPI_PORT0,RLatch[2]);
        delay_cycles(3);
  set_tris_a(0b11101111);
  output_high(PIN_A5);
  delay_cycles(20);
  output_low(PIN_A5);


  //write the NCounterLatch
  spi_xfer(SPI_PORT0,NCounterLatch[0]);
        delay_cycles(3);
  spi_xfer(SPI_PORT0,NCounterLatch[1]);
        delay_cycles(3);
  spi_xfer(SPI_PORT0,NCounterLatch[2]);
        delay_cycles(3);
  set_tris_a(0b11101111);
  output_high(PIN_A5);
         delay_cycles(3);
  output_low(PIN_A5);
      delay_cycles(20);

  //enable the PLL
  output_high(PIN_C2);



}


void IAmAlive()
{     //set_tris_a(0b11111011);
      output_toggle(PIN_A2);
      //delay_ms(500);

}
```

```
void readADC(long* PtrAMPadcResult, long* PtrPMadcResult)
{       int const N = 5;
        long AMPadc[N];
        long PMadc[N];
        int i;

        for (i = 0; i<=N-1 ; i++)
        {


            set_adc_channel(0);
            delay_us(2000);
            PMadc[i] = read_adc();
            set_adc_channel(1);
            delay_us(2000);
            AMPadc[i] = read_adc();
        }

        //average the ADC readings

        for (i = 0; i<=N-1; i++)
        {
         *PtrAMPadcResult += AMPadc[i];
         *PtrPMadcResult += PMadc[i];
        }

        *PtrAMPadcResult = *PtrAMPadcResult/N;
        *PtrPMadcResult = *PtrPMadcResult/N;
}
```